Optimization of UAV Propeller for Enhanced Efficiency and Noise Reduction

Fazley Rabby Patwary

ID: 21107013

DEPARTMENT OF MECHANICAL ENGINEERING

COLLEGE OF ENGINEERING AND TECHNOLOGY

IUBAT—INTERNATIONAL UNIVERSITY OF BUSINESS AGRICULTURE AND TECHNOLOGY

Spring, 2025

Optimization of UAV Propeller for Enhanced Efficiency and Noise Reduction

By

Fazley Rabby Patwary

ID: 21107013

Program: BSME

A THESIS SUBMITTED IN PARTIAL FULFILMENT OF THE REQUIREMENTS FOR THE DEGREE,

BACHELOR OF SCIENCE IN MECHANICAL ENGINEERING (BSME)

DEPARTMENT OF MECHANICAL ENGINEERING

COLLEGE OF ENGINEERING AND TECHNOLOGY

IUBAT—INTERNATIONAL UNIVERSITY OF BUSINESS AGRICULTURE AND TECHNOLOGY

DECLARATION

This thesis has been prepared after twelve months of research on "**Optimization of UAV Propeller for Enhanced Efficiency and Noise Reduction**". The thesis is solely for the academic requirement of the course MEC 488 and has not been submitted in part or full elsewhere for any other degree, reward, or any other purpose. We do solemnly declare that all and every right in the copyright of this thesis belongs to IUBAT-International University of Business Agriculture and Technology. Any reproduction or use in any form or by any means whatsoever is prohibited without the written consent of IUBAT.

Fazley Rabby Patwary

ID: 21107013

ACKNOWLEDGMENT

First of all, we would like to express our gratitude to our honourable supervisor Dr. Debasish Sarker, Assistant Professor, Department of Mechanical Engineering for his guidance and contribution to our work. Our thesis is the result of his support and effort.

We sincerely acknowledge the contributions of Professor and Chair Dr. Dewan Mohammad Nuruzzaman, Associate Professor and Coordinator Dr. A. K. M. Parvez Iqbal, Department of Mechanical Engineering at IUBAT-International University of Business Agriculture and Technology for continuous support to come up with a thesis.

We would like to express our gratitude to the jury for their thoughtful comments which helped us to enrich our thesis project. We also acknowledge the contributions of our faculties at IUBAT-International University of Business Agriculture and Technology for their cooperation, support, and motivation that enabled us to complete our thesis.

Special thanks to former student Md. Motiur Rahman, whose contributions helped make this thesis turn into a reality. We are also grateful to IIEC for providing 3D printing service.

We would also like to thank our parents, family members, friends and relatives for their cooperation, affection, and help throughout attending this study. Their support in hard times and motivation to keep doing hard work constantly, helped us a lot to come up with this good work.

Fazley Rabby Patwary

ID: 21107013

Optimization of UAV Propeller for Enhance Efficiency and Noise Reduction

Candidates

Fazley Rabby Patwary

ID: 21107013

Supervisor

Dr. Debasish Sarker

Department of Mechanical Engineering

ABSTRACT

Unmanned Aerial Vehicles (UAVs) are becoming an essential part of modern industries, from aerial surveillance and package delivery to agricultural monitoring. However, one of the biggest challenges in UAV design is the noise generated by their propellers, which can be disruptive in urban areas and military operations. At the same time, improving energy efficiency is crucial for extending flight time, especially for battery-powered UAVs. This study explores an innovative approach to optimizing UAV propeller design to reduce noise and enhance aerodynamic efficiency using a combination of Computational Fluid Dynamics (CFD), Blade Element Momentum Theory (BEMT), and Genetic Algorithm (GA)-based optimization.

By applying GA-driven optimization, this research fine-tunes key propeller parameters, including chord length to maximize efficiency while minimizing energy consumption. CFD simulations using ANSYS Fluent help analyze airflow, vortex formations, and noise sources, while the Ffowcs-Williams/Hawkings (FW-H) model predicts aeroacoustic behavior. To validate these computational results, 3D-printed versions of the optimized and baseline propellers were experimentally tested for thrust, torque, power usage, and noise levels.

The findings show that the optimized propeller achieves a 4-5% improvement in thrust-to-torque ratio, meaning it generates the same thrust while using less power. Additionally, tonal noise at the Blade Passing Frequency (BPF) is reduced by 1.5-2 dB, making the UAV quieter without sacrificing performance. These results demonstrate that small design changes, such as blade tip modifications, can significantly enhance UAV efficiency and noise control, leading to longer flight times and greater acceptance in noise-sensitive environments.

LIST OF ABBREVIATIONS

RANS	Reynolds-Averaged Navier-Stokes
CFD	Computational Fluid Dynamics
RPM	Revolutions Per Minute
MRF	Moving Reference Frame
BET	Blade Element Theory
BEMT	Blade Element Momentum Theory
SA	Spalart Allmaras
DM	Design Modeler
UAV	Unmanned Aerial Veichle
GA	Genetic Algorithm
FW-H	Ffowcs-Williams/Hawkings
CAA	Computational Aeroacoustics
SPL	Sound Pressure Level

LIST OF SYMBOLS

Symbol	Definition	Unit
C	Chord	m
C_d	Coefficient of Drag	-
C_L	Coefficient of Lift	-
D	Drag Force	N
f_{BPE}	Blade Pass Frequency	Hz
L	Lift Force	N
N	Number of Blades	-
P_i	Induced Power/ Aerodynamic Power	W
Q	Torque	Nm
r	Radial Distance from Centre	m
T	Fitness Function	-
V_{up}	Vertical velocity of the UAV during takeoff	m/s
V_i	Induced velocity due to the propeller's airflow	m/s
W	Relative Velocity at Blade	m/s
α	Angle of Attack	$Degree$
β	Air Inlet Angle at Blade	$Degree$
ρ	Density	Kg/m^3
$\dot{m}$	Mass Flow Rate	kg/m^3
$\dot{M}_r$	rate of change of Mach number	s^{-1}
δ	Pitch Angle	$Degree$
Ω	Angular Velocity	rad/s
ϕ	Hub to Tip Ratio	-
λ	Induced Velocity	-

Table of Contents

List of the Figures

List of the Tables

CHAPTER 1: INTRODUCTION

1.1 Research Background

Unmanned Aerial Vehicles (UAVs) have become a transformative technology, with applications spanning military, commercial, and industrial sectors. Their ability to perform tasks such as surveillance, infrastructure inspection, and short-distance delivery with high maneuverability and rapid deployment has driven their widespread adoption [1]-[2]. The global UAV market, valued at $26.9 billion in 2022, is projected to grow at a compound annual growth rate (CAGR) of 17.4% from 2023 to 2030, driven by advancements in sensing, control technologies, and increasing demand for efficient aerial solutions [3].

The performance of UAVs is heavily influenced by their propulsion systems, particularly the propellers, which determine thrust, drag, power efficiency, and noise levels [4]. For electric-powered UAVs, energy efficiency is critical due to the limitations of battery capacity, which directly impacts flight duration and operational effectiveness [5]. Optimizing propeller design to maximize thrust while minimizing energy consumption is essential for extending flight times and improving overall performance [6].

Recent advancements in computational techniques, such as Computational Fluid Dynamics (CFD) and Blade Element Momentum Theory (BEMT), have enabled the analysis and optimization of propeller designs. These tools allow for the exploration of various blade shapes, pitch angles, and chord distributions to achieve higher aerodynamic efficiency [7]-[8]. Additionally, optimization algorithms like Genetic Algorithms (GA) have proven effective in refining propeller geometry to balance performance metrics such as thrust, torque, and noise [9]. However, UAV propellers also face challenges related to noise generation, particularly in urban environments and military applications. Propeller noise, often exceeding 60-80 dB at close range, can disrupt operations and pose regulatory challenges [11]. Addressing these issues without compromising aerodynamic performance is crucial for expanding UAV applications in noise-sensitive areas [12]-[13].

This research focuses on optimizing UAV propeller design to improve aerodynamic efficiency and reduce noise emissions through a combination of GA-based optimization, CFD simulations, and experimental validation. By combining these tools, the study aims to develop propellers that

enhance UAV performance while addressing the growing demand for quieter and more efficient aerial vehicles.

1.2 Problem Statement and Significance

Despite significant advancements in UAV technology, improving the energy efficiency and noise levels of UAV propellers remains a critical challenge. Propeller geometry directly influences thrust, drag, power consumption, and noise emissions, making it a key factor in UAV performance [4], [14]. Optimizing these properties can enhance thrust generation while reducing energy consumption, which is especially crucial for electric-powered UAVs where battery life is a limiting factor [5], [15].

Noise generation is another major limitation, particularly for UAVs operating in urban environments or military surveillance missions. Excessive noise can compromise mission success, pose regulatory challenges, and hinder public acceptance [16]-[17]. Propeller noise primarily arises from turbulent flow interactions at the trailing edge and tip, as well as blade vortex interactions [18]. Reducing noise without compromising aerodynamic performance is essential for expanding UAV applications in noise-sensitive areas [19]-[21].

This study addresses these challenges by combining Genetic Algorithm (GA)-based aerodynamic optimization with passive noise mitigation techniques, such as tip modifications. The research aims to develop UAV propeller designs that improve thrust output and efficiency while minimizing noise, enabling better performance in noise-restricted environments. By leveraging CFD simulations and experimental validation, this study provides a comprehensive framework for optimizing UAV propellers, enhancing their energy efficiency and noise control capabilities.

The significance of this research is underscored by the following factors:

- Growing Demand for Efficient UAVs: The increasing use of UAVs in commercial and industrial applications, such as delivery services and agricultural monitoring, necessitates more efficient propulsion systems. For example, a 10% improvement in propeller efficiency can lead to a 15-20% increase in flight time for battery-powered UAVs [23].
- Noise Reduction for Urban Integration: Noise pollution is a major barrier to the widespread adoption of UAVs in urban areas. Quieter propellers are essential for regulatory

compliance and public acceptance, particularly for applications like drone delivery and urban surveillance [22].

- Technological Advancements: The availability of advanced computational tools (e.g., CFD, BEMT) and optimization algorithms (e.g., genetic algorithms) enables the exploration of novel propeller designs. Additionally, 3D printing technology allows for rapid prototyping and experimental validation of optimized designs [24, 25].
- Real-World Impact: Improved propeller designs can have a significant impact on industries such as agriculture, where UAVs are used for crop monitoring and spraying. For example, a 20% increase in propeller efficiency could reduce operational costs by $1-2 per acre for agricultural drones [28].

1.3 Objectives

1. Develop a Genetic Algorithm using BEMT to optimize blade twist, chord length, and airfoil shape for maximum efficiency.
2. Use CFD to analyze flow, thrust, and power, and compare results with BEMT predictions.
3. 3D print optimized and baseline propellers, then test thrust, power, and noise experimentally.
4. Compare optimized propellers with APC 8045 to quantify efficiency and noise improvements.

1.4 Organization of the Report

This report is organized into six chapters:

Chapter 1: Introduction: Provides the research background, problem statement, significance, and objectives of the study.

Chapter 2: Literature Review: Reviews existing research on UAV propeller design, aerodynamic optimization, and noise reduction techniques.

Chapter 3: Theoretical Background: Discusses the theoretical foundations of aerodynamics, Blade Element Momentum Theory (BEMT), and Computational Fluid Dynamics (CFD) used in this study.

Chapter 4: Methodology: Describes the research methodology, including the genetic algorithm optimization process, CFD simulations, model validation and experimental setup.

Chapter 5: Results and Discussion: Presents the findings of the study, including aerodynamic performance, noise reduction.

Chapter 6: Conclusion and Recommendations: Summarizes the key findings, contributions, and limitations of the study, and provides recommendations for future work.

1.5 Limitations of the Report

While this study provides valuable insights into the optimization of UAV propellers, it has certain limitations:

1. Scope of Tip Modifications: The study focused on specific tip modifications for noise reduction. Future work could explore a wider range of geometric changes to further improve aerodynamic efficiency and noise reduction.
2. Experimental Constraints: The experimental validation was conducted in a controlled environment. Real-world conditions, such as wind gusts and turbulence, were not fully replicated, which may affect the generalizability of the results.
3. Material Limitations: The 3D-printed propellers were made from PLA+ filament, which may not fully represent the performance of propellers made from advanced materials like carbon fiber composites.
4. Computational Resources: The CFD simulations were limited by computational resources, which restricted the mesh resolution and simulation time. Higher-fidelity simulations could provide more detailed insights into flow dynamics and noise generation.
5. Structural Analysis: The study did not consider the structural implications of the optimized designs, such as vibration and fatigue. Future work could incorporate structural analysis to ensure the durability and reliability of the propellers.

CHAPTER 2: LITRATURE REVIEW

2.1 Literature Survey

The design of UAV propellers has seen rapid progress in recent years, with researchers focusing on improving aerodynamic efficiency, optimizing geometry, and reducing noise. Fundamental modeling approaches like Blade Element Theory (BET) and Blade Element Momentum Theory (BEMT) have been widely used to understand how factors such as blade pitch, diameter, curvature, and angle of attack influence overall performance. These methods offer valuable insights into how propellers generate thrust and respond to different operating conditions [4]-[5].

Beyond the basics, many studies have explored innovative design tweaks to enhance propeller performance. For instance, introducing sinusoidal leading edges or serrated trailing edges has shown promise in boosting lift and delaying stall, while also helping to manage noise levels [6]-[7]. These design ideas can now be tested and refined more easily and cost-effectively than before [8].

Optimization has also become a major focus, especially with the help of algorithms like Genetic Algorithms (GA), Particle Swarm Optimization (PSO), and Differential Evolution (DE) [9]. These methods are being used to fine-tune blade geometry, improve motor-propeller integration, and push the limits of aerodynamic performance [10]. Some frameworks even combine these algorithms with theoretical models and simulation tools to create more comprehensive design solutions [11].

Noise reduction, a key concern for UAVs operating in urban or sensitive areas, has also been addressed through both numerical simulations and experimental testing [12]. Techniques like trailing-edge serrations and winglet modifications have been shown to effectively cut down on broadband and tonal noise, all while preserving or even improving aerodynamic performance [13]-[14].

These studies highlight the importance of a well-rounded design approach—one that balances aerodynamic efficiency, structural considerations, and acoustic performance. As UAV applications continue to grow, these integrated strategies will play a crucial role in developing quieter, more capable, and more efficient systems.

CHAPTER 3: THEORETICAL BACKGROUND

Aerodynamics is the fundamental study of understanding how air moves around an object, and of course, such studies are especially important to UAV propeller design. The performance of an aircraft or UAV is decided by forces like lift, drag, thrust and weight. These forces are calculated based on fluid dynamics, the principle of which is that air behaves like the continuum medium where the properties such as velocity, pressure, and density vary smoothly all over the space and time.

Normally three fundamental conservation principles are used for analyzing the aerodynamic performance.

1. Conservation of Mass (Continuity Equation)
2. Conservation of Momentum (Newton's Second Law)
3. Conservation of Energy (First Law of Thermodynamics)

3.1 Conservation of Mass (Continuity Equation)

The continuity equation ensures that mass is neither created nor destroyed in a flow field. This principle states that the mass flow rate remains constant along a streamline:

$$\dot{m} = \rho A V \qquad (1)$$

Where:

$\dot{m}$ = mass flow rate
ρ = fluid density
A = cross-sectional area
V = velocity of airflow

Differential Form, $\nabla \cdot (\rho \mathbf{V}) = 0$ (2)

This principle is crucial for analyzing UAV propeller airflow, as it determines how air is accelerated through the propeller disk.

3.2 Conservation of Momentum

This principle, derived from Newton's Second Law, states that any change in momentum within a fluid flow is due to external forces. These forces can be surface forces, such as frictional (viscous) forces, or body forces, such as gravitational effects. The momentum conservation law can be expressed either as a vector equation or as three separate scalar equations representing the components along the x, y, and z directions:

$$\rho \frac{Du}{Dt} = -\frac{\partial p}{\partial x} \tag{3}$$

$$\rho \frac{Dv}{Dt} = -\frac{\partial p}{\partial y} \tag{4}$$

$$\rho \frac{Dw}{Dt} = -\frac{\partial p}{\partial z} \tag{5}$$

Where, ρ is the fluid density, p is the pressure, u, v, w are the velocity components in the x, y, and z directions, respectively.

3.3 Conservation of Energy

According to the First Law of Thermodynamics, energy cannot be created or destroyed in a flow field. Instead, any variation in energy within a given control volume results from either heat transfer or work done on or by the fluid. This principle is mathematically expressed as:

$$\rho \frac{D(e + V^2/2)}{Dt} = \rho \dot{q} - \nabla \cdot (\rho \mathbf{V}) \tag{6}$$

Where:

- e represents the internal energy per unit volume,
- V is the velocity of the fluid element,
- q˙ is the volumetric heat addition rate,
- D/Dt is the total (material) derivative, given by

$$\frac{D}{Dt} = \frac{\partial}{\partial t} + (\mathbf{V} \cdot \nabla)$$

This equation accounts for both local changes in energy over time and convective changes due to fluid motion.

3.4 Aerodynamic Forces

Many forces act on bodies submerged in air, these are called aerodynamic forces e.g. lift, drag, thrust, etc. Among these forces, we will focus on lift and drag. To give visual representation a figure 1 is added-

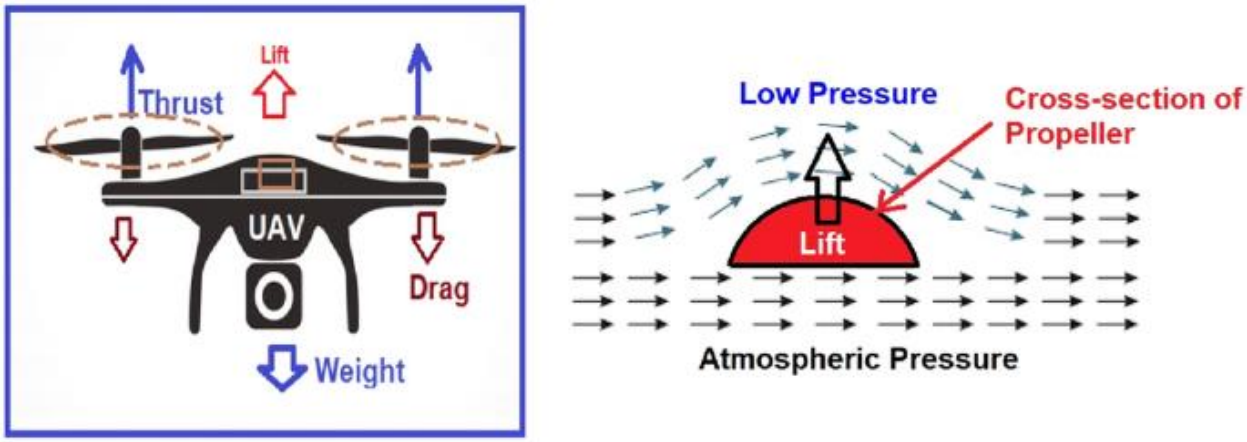

Figure 1: Aerodynamic Forces Acting on a UAV [22].

3.4.1 Lift Force

A fluid flowing around an object exerts a force on it. Lift is the component of this force that is perpendicular to the oncoming flow direction [23].

Lift,

$$L = \frac{1}{2} C_l \rho A V^2 \quad (7)$$

Or,

$$L = \frac{1}{2} C_l \rho C b V^2 \quad (8)$$

Here, L is lift force on the blade; C_l is the coefficient of lift; ρ is the density of the fluid; A is the area of the blade C times b, where C is the chord and b is the span; V is the velocity of incoming air; and α is the angle of attack.

3.4.2 Drag Force

Aerodynamic drag force is defined as the force that is faced by the vehicle as it moves through the air [24].

Drag,

$$D = \frac{1}{2} C_d \rho A V^2 \quad (9)$$

Or,

$$D = \frac{1}{2} C_d \rho C b V^2 \quad (10)$$

Here, D is drag force on the blade; C_d is the coefficient of drag; ρ is the density of the fluid; A is the area of the blade C times b, where C is the chord and b is the span; V is the velocity of incoming air; and α is the angle of attack.

3.4.3 Coefficient of Lift

The coefficient of lift is a non-dimensional number associated with lift force. It is an experimental value, and it is a function of the angle of attack for a given shape.

Coefficient of Lift,

$$C_l = \frac{L}{\frac{1}{2} \rho A V^2} \quad (11)$$

Or,

$$C_l = \frac{L}{\frac{1}{2} \rho C b V^2} \quad (12)$$

3.4.4 Coefficient of Drag

The coefficient of drag is a non-dimensional number associated with drag force. It is an experimental value, and it is a function of th-e angle of attack for a given shape.

Coefficient of Drag**,**

$$C_d = \frac{D}{\frac{1}{2} \rho A V^2} \quad (13)$$

Or,

$$C_d = \frac{D}{\frac{1}{2} \rho C b V^2} \quad (14)$$

These forces contribute to the overall thrust and torque produced by the propeller. The torque is required to overcome the resistive drag, and it plays a key role in power consumption. As modifications like serrations and tip reductions are applied, changes in these aerodynamic forces must be evaluated to ensure that thrust is not compromised.

3.4.5 Blade Element Momentum Theory for UAV Propeller Analysis

BEMT is a fundamental method for predicting the aerodynamic performance of propellers by combining BET and Momentum Theory. BET divides the propeller blade into multiple small segments (or elements), treating each element as an independent airfoil and analyzing the aerodynamic forces acting on it. Momentum Theory, on the other hand, provides a global view of how the propeller affects the surrounding airflow by considering conservation of momentum. By integrating these two approaches, BEMT allows for the calculation of thrust, torque, and power requirements, which are essential for optimizing UAV propulsion systems. Figure 2 shows the propeller different section to calculate BET.

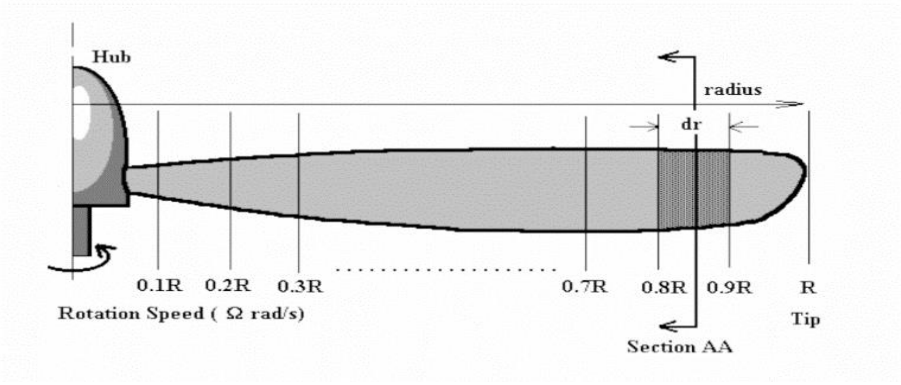

Figure 2: Different section for analyzing BEMT [25].

Theoretical Foundation of BEMT

A UAV propeller consists of multiple rotating blades, each of which experiences different aerodynamic forces along its length. The performance of the propeller is determined by the combined contributions of all blade elements.

The parameters, velocities, and forces of a blade element are shown in Figure 3, where V_{up} is the speed at which the drone takes off vertically, V_i is the induced velocity, $\Omega \cdot r$ is the linear velocity of the blade element at the position where the radius is r, at the axis of the propeller, r = 0, the linear velocity is 0, and the tip of the propeller is r = R, the linear velocity is $\Omega \cdot R$, where Ω is the rotor angular velocity and R is the propeller radius, W is the relative air velocity, α is the angle of attack, φ is the pitch angle, and ε is the inflow angle.

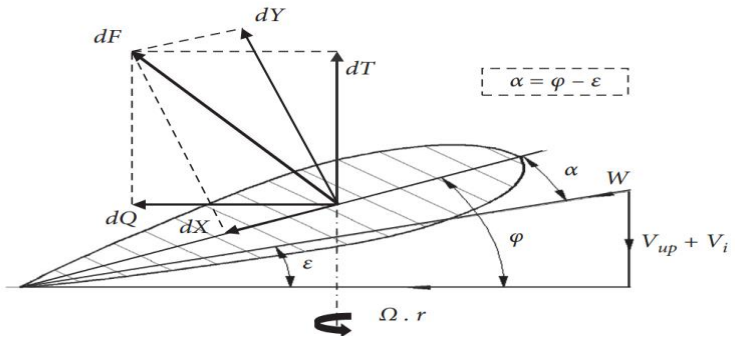

Figure 3: Parameters, Velocities, and Forces of a Blade Element [26].

Relative Velocity of a Blade Element

Each blade element moves through the air with a combination of axial velocity caused by UAV motion and induced airflow and tangential velocity caused by the propeller's rotation. The velocity W at a blade element is given by:

$$W = (V_{up} + V_i) + \Omega_r \quad (15)$$

Where:

- V_{up} = Vertical velocity of the UAV during takeoff
- V_i = Induced velocity due to the propeller's airflow
- Ω = Angular velocity of the propeller (rad/s)
- r = Radial distance of the blade element from the center of rotation

The inflow angle ε of the airflow at the blade element is determined by:

$$\varepsilon = \tan^{-1}\left(\frac{(V_{up} + V_i}{\Omega_r}\right) \tag{16}$$

This inflow angle affects the local angle of attack α and, consequently, the aerodynamic forces generated by the blade.

Aerodynamic Forces on a Blade Element

Aerodynamic performance mainly refers to the lift, resistance, and power generated by the blade during the working process. The coefficient of lift and drag, C_l and C_d, are needed to calculate the lift and drag generated by blades according to blade element momentum theory.

$$C_l = \frac{Y}{\frac{1}{2}\rho W^2 S} \tag{17}$$

$$C_d = \frac{X}{\frac{1}{2}\rho W^2 S} \tag{18}$$

Where:

- ρ = air density
- W = local relative velocity at the blade element
- C_l = lift coefficient of the airfoil
- C_d = drag coefficient of the airfoil
- X = airfoil drag
- Y= airfoil lift
- S = elemental blade area

S can be calculated according to

$$S = b \cdot \Delta r \tag{19}$$

Where b is the length of the chord and Δr is the length of the blade element. Cl and Cd are determined for the lift and resistance curves, respectively, according to α and the Reynolds number, Re:

$$R_e = \frac{\rho v_f l}{\mu} \tag{20}$$

Where v_f is the freestream velocity, μ is the kinetic viscosity, and l is the characteristic dimension, which is usually defined as either local chord length or chord length at 75% of radius. Therefore, the differential lift of the element, dY, and drag of the element, dX, can be calculated as-

$$dY = \left(\frac{1}{2}\rho W^2 C_l b\right) dr \tag{21}$$

$$dX = \left(\frac{1}{2}\rho W^2 C_d b\right) dr \tag{22}$$

These aerodynamic forces act at an angle, contributing to both thrust (T) along the rotation axis and torque (Q), which resists the rotation of the propeller. The differential contributions to thrust and torque from each blade element are:

$$dT = \cos(\varepsilon) dY - \sin(\varepsilon) dX \tag{23}$$

$$dQ = \sin(\varepsilon) dY + \cos(\varepsilon) dX \tag{24}$$

Where, ε is the inflow angle.

The total thrust and torque of the propeller are obtained by integrating over all blade elements along the radius:

$$T = \int_{r_o}^{r_{tip}} dT \tag{25}$$

$$Q = \int_{r_o}^{r_{tip}} dQ \tag{26}$$

Where r_o is the root radius (inner section of the blade) and r_{tip} is the tip radius of the blade.

3.4.6 Thrust and Torque Relationship in UAV Propellers

Thrust and torque in UAV propellers are directly related through aerodynamic efficiency and power consumption. The torque Q required to rotate a propeller is given by:

$$Q = \int_{R_i}^{R_{tip}} r dD \tag{27}$$

Where, R_i and R_{tip} are the inner and outer radius of the propeller, respectively. This equation shows that increasing the drag on the blades leads to a higher torque requirement, which in turn increases power consumption. To optimize UAV efficiency, a balance must be maintained between thrust generation and torque requirements.

3.5 Noise Sources in UAV Propellers

Propeller noise is composed of tonal and broadband components. Sources of propeller aerodynamic noise are shown in Fig. 4 and 5 shows noise classifications of propeller and UAVs total noise sources.

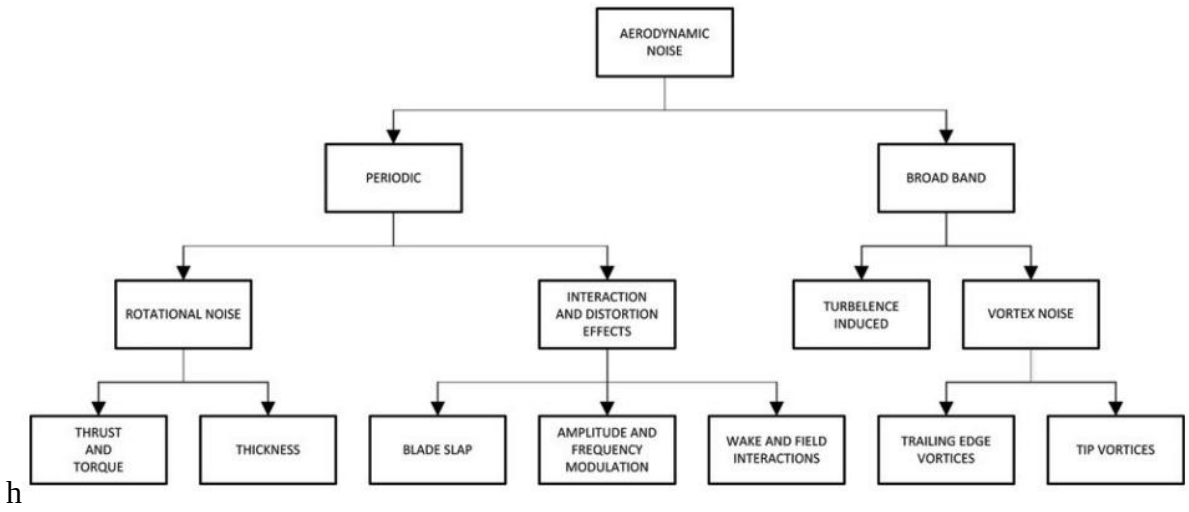

h

Figure 4: Propeller Noise Classification [29].

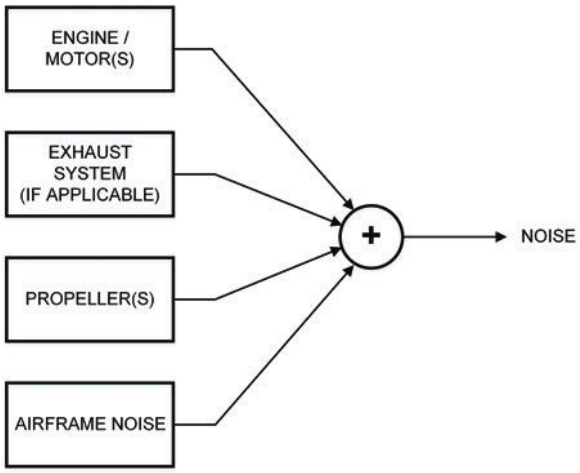

Figure 5: UAV Noise Sources [29].

The greatest noise, in terms of directivity, is in the propeller plane. The basic frequency f_1 or f_{BPF} (Blade Pass Frequency), is the product of the propeller rotational speed and the number of propeller blades [27]:

$$f_1 = f_{BPF} = \frac{Nrpm \cdot Nb}{60} \tag{28}$$

Where, f_{BPF} is the basic frequency of tonal propeller component, Nrpm is the propeller rotational speed, harmonics $f_n = N \cdot f_1$, and Nb is the number of propeller blades. In fig 6, the tonal components contain basic frequency f_1 and its harmonics f_n with spectral components has shown.

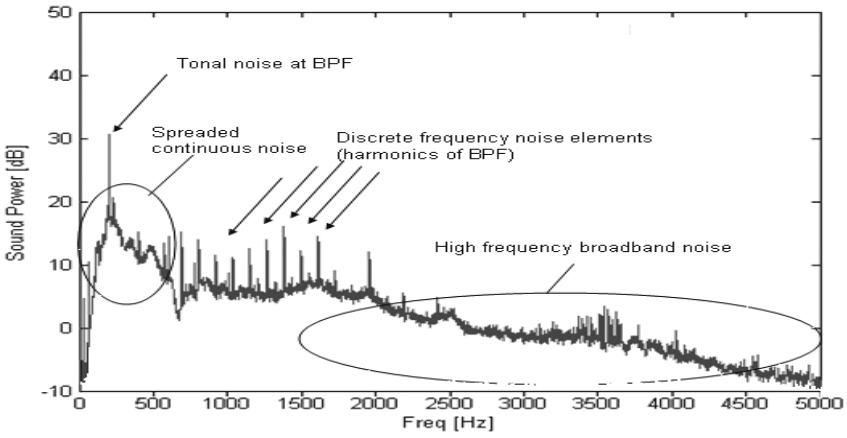

Figure 6: Tonal Components and Spectral Analysis of UAV Propeller [26].

3.6 Boundary Layer Separation and Noise Generation in UAV Propellers

Boundary layer separation plays a critical role in UAV propeller noise generation, particularly in trailing edge noise and vortex shedding. When airflow over a propeller blade fails to remain attached to the surface due to adverse pressure gradients, it leads to turbulent wake formation, significantly increasing aero acoustic emissions.

3.6.1 Boundary Layer and Separation Mechanism

The boundary layer is the thin layer of air near the surface of a propeller blade where viscous forces dominate. It can be classified into:

- **Laminar boundary layer:** Smooth, orderly flow with minimal energy dissipation.
- **Turbulent boundary layer:** Chaotic, high-energy flow with increased skin friction.

3.6.2 Flow Separation Condition

Boundary layer separation occurs when adverse pressure gradients (APG) cause the airflow to reverse direction, detaching from the blade surface. The separation point is determined by:

$$\frac{du}{dy} = 0 \tag{29}$$

Where u is the flow velocity parallel to the surface, and y is the distance from the surface.

Figure 7 shows the flow separation region of the propeller where laminar flow transform into turbulent and contribute in overall noise generation.

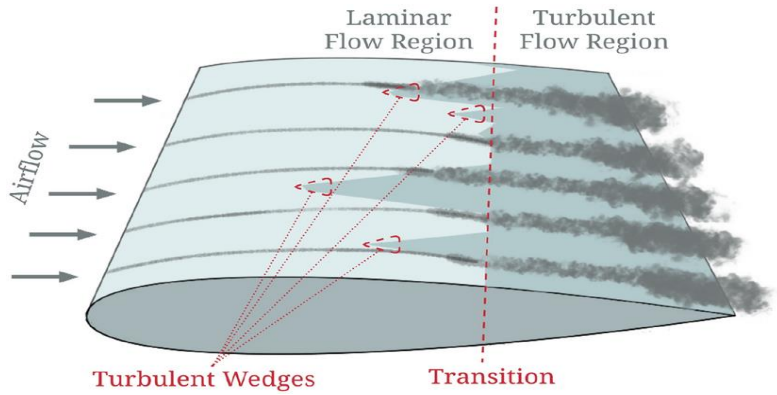

Figure 7: Boundary Layer Flow Separation of the Propeller [11].

3.6.3 Noise Generation Due to Boundary Separation

A thicker separated boundary layer leads to higher noise levels, which is why serrated trailing edges help by disrupting coherent turbulence structures. At higher Reynolds numbers, vortex shedding becomes more intense, increasing propeller noise emissions. Figure 8 shows how the flow separated and create vortex in airfoil.

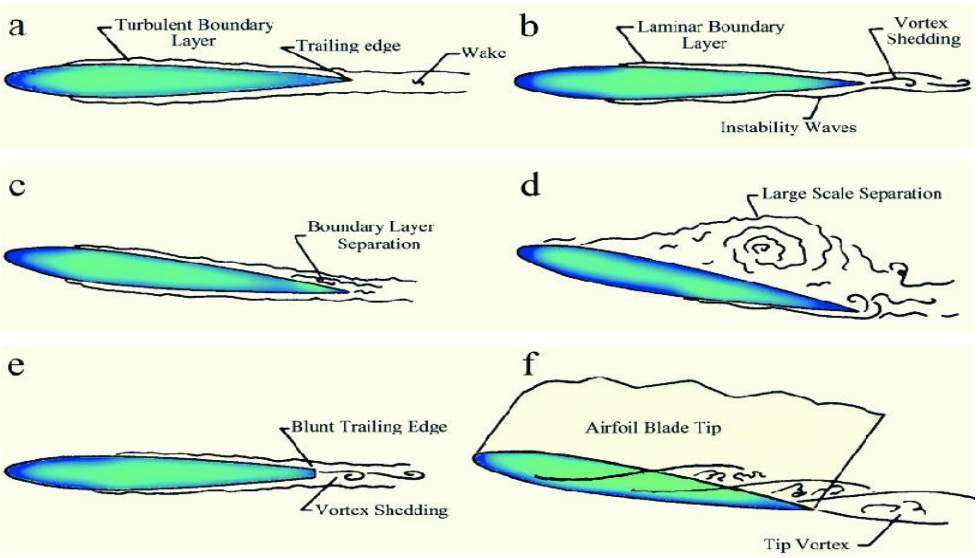

Figure 8: Vortex-shedding for Boundary Layer Separation [27].

3.6.3 Noise Reduction Strategies Related to Boundary Layer Control

Several design modifications can be made to reduce noise due to the boundary layer separation. Trailing edge serrations disrupting turbulence structures as well as diffusing pressure fluctuations, by this way it smaller and less powerful eddies and minimizing broadband noise. This mechanism is inspired from the glowing feathers in owls that allow it to be silent. Smooth coatings on the blade surface reduce the skin friction and delay the flow separation; riblets improve an attachment of boundary layer, which decreases noise levels. Also, tip modifications (such as swept and rounded tips) will weaken tip vortex strength, which will indirectly reduce separation-induced noise and enhance overall aerodynamic performance. Reduction in the tip area specifically reduces tonal noise due to reduced vortex strength at the tip; studies suggest that reducing the tip radius by 5–8% can reduce tonal noise very effectively [7].

3.7 FW-H Equation for Propeller Noise

The Ffowcs-Williams/Hawkings (FW-H) equation is widely used to calculate the noise signature of rotating blades, such as UAV propellers. It is derived from the constrained wave equation and incorporates different noise-generating mechanisms. The general form of the FW-H equation is [29]:

$$\frac{1}{a^2}\frac{\partial^2 p}{\partial t^2} - \nabla^2 p = \frac{\partial^2 T_{ij}}{\partial x_i \partial x_j} + \frac{\partial}{\partial t}\left[\delta(f)(v_i \frac{\partial f}{\partial x_i} + p_{ij}\frac{\partial f}{\partial x_j}\right] \quad (30)$$

Where, a = speed of sound, p = perturbation in static pressure, T_{ij} = Lighthill stress tensor, p_{ij} = generalized stress tensor, v_i = source velocity vector, f (x) = function defining the surface generating the pressure wave.

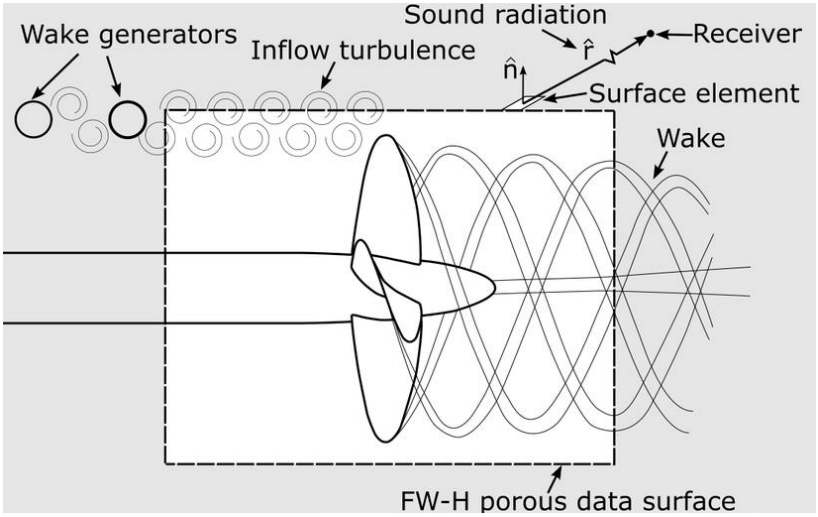

Figure 9: Fw-h Noise Model on Data Surface [28].

This equation considers *three forcing terms* that contribute to propeller noise:

1. **Thickness noise:** Due to the displacement of air by rotating blades.
2. **Loading noise:** Resulting from unsteady aerodynamic forces on the blades.

For thin propeller blades operating at subsonic or transonic speeds, the vortex noise term is often neglected, simplifying the equation to focus on thickness and loading noise components.

The total noise pressure p(x, t) is then given as:

$$P(x, t) = P_{thick}(x, t) + P_{loading}(x, t) \quad (31)$$

Where, P_{thick} is represents thickness noise, and $P_{loading}$ represents is loading noise.

3.7.1 Approximate Noise Models for UAV Propellers

To solve the FW-H equation, several assumptions are made for computational feasibility [29]:

1. The noise source velocity is subsonic (M<1).
2. The observer is stationary relative to the source.
3. The propeller rotation speed and UAV velocity are constant over time.

Applying these assumptions, the expressions for loading noise and thickness noise become:

(a) Loading Noise Equation

$$P_{loading}(x, t) = \frac{1}{4\pi}\sum_k \left[\frac{\dot{F}\cdot r_{rel}+F\cdot M}{r_{rel}\,(1-M_r)}\right]_{far-feild} + \left[\frac{F\cdot M}{r_{rel}^2(1-M_r)}\right]_{near-feild} \quad (32)$$

Where, F = aerodynamic force per element, r_{rel} = relative position vector between observer and noise source, M = Mach number vector (v/a), M_r = projection of M onto r_{rel}.

The far-field noise scales as $\frac{1}{r_{rel}}$ while the near-field noise scales as $\frac{1}{r_{rel}^2}$. So that, at large distances, the near-field contribution becomes negligible.

(b) Thickness Noise Equation

$$P_{thick}(x, t) = \frac{1}{4\pi}\sum_k \left[\frac{\dot{M}_r+M}{(1-M_r)^3}\right] \quad (33)$$

Where, $\dot{M}_r$ = rate of change of Mach number.

Thickness noise is typically lower in magnitude than loading noise but dominates at high rotational speeds.

3.8 Spectral Analysis of UAV Propeller Noise

Once the pressure wave p(x, t) is determined, its frequency components can be analyzed using Fourier Transforms. The sound pressure level (SPL) is calculated as [29]:

$$SPL = 10 \log_{10}\left(\frac{p^2}{p_{ref}^2}\right) \tag{34}$$

Where, P_{ref} =20×10−6 Pa (reference sound pressure for air).

Figure 10 shows the harmonic noise peaks are consists of tonal noise, so the most annoying noise is the tonal noise itself.

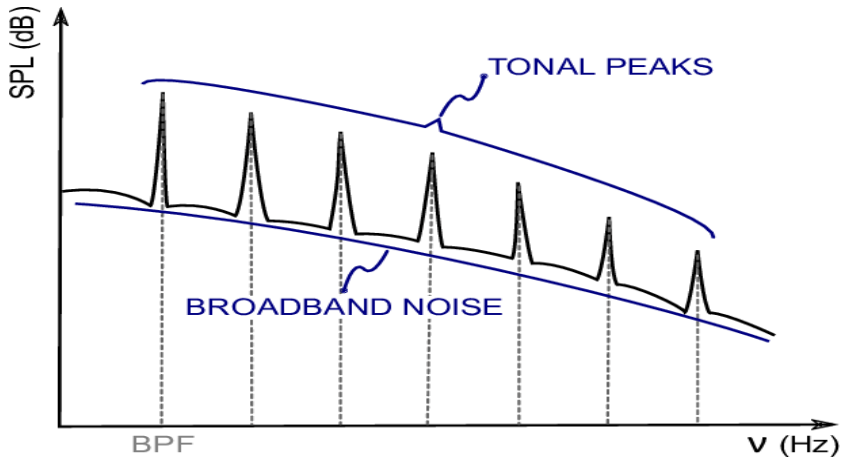

Figure 10: Comparison between Tonal and Broadband Noise in a Harmonic Component [29].

The harmonic components of noise are extracted using the Fast Fourier Transform (FFT):

$$P_{FFT,\,i} = \frac{1}{T_c}\int_0^{T_c} p^2(x,t)dt \tag{35}$$

Where T_C is the duration of one noise cycle (equivalent to half a revolution for a two-bladed propeller. The A-weighted sound pressure level (SPLA), which considers human hearing sensitivity, is defined as:

$$SPLA = SPL + dBA(f) \tag{36}$$

Where dBA (f) is an empirical weighting function that adjusts SPL values based on perceived loudness at different frequencies [29].

3.9 Practical Implications for UAV Noise Reduction

By Using spectral analysis in combination with the FW-H equation engineers can identify dominant noise sources like thickness noise at high RPMs and loading noise in maneuvers to target which noise reduction strategy should be applied. These equation help to find out the optimal propeller blades design which increases the propellers aeroacoustics performance like to reduce the tonal noise, adjustments to blade pitch, aspect ratio, and tip geometry and these are used to make UAV's quieter and more efficient [29].

3.10 Evolutionary Theory of Design

Evolutionary theory was inspired by natural selection, and can be widely applied in field of aerospace, fluid dynamics and structural design, including engineering optimization. The aerodynamic efficiency, noise reduction, and structural integrity are evaluated for generations of design variations generated from techniques such as Genetic Algorithms and Evolutionary Strategies, performance of which is determined, and best configurations selected. Some equivalent tradeoffs facilitated by a multi objective evolutionary approach such as NSGA-II, are drag reduction, lift enhancement, and the weight minimization. Evolutionary methods have been successfully applied to aerodynamic surface refinement via generation of more efficient aerodynamic surfaces for airfoil optimal shape, wind turbine blade refinement, and aero acoustic analysis. Bio inspired aerodynamic design still uses evolutionary principles to conquer further and increase bio inspired aerodynamic design toward the next generation aircraft, rotorcraft and propulsion with better performances and noise control [10].

CHAPTER 4: METHODOLOGY

In this chapter, the detailed process of the thesis work is discussed. Firstly, the analytical calculation is done to get thrust and torque results, then based on the theory a python based computer programmed genetic algorithm is introduced. Secondly, to verify the algorithm results, propellers CFD simulation is done by using Ansys student version R2 2024. Finally, by doing experiment real world application is validated.

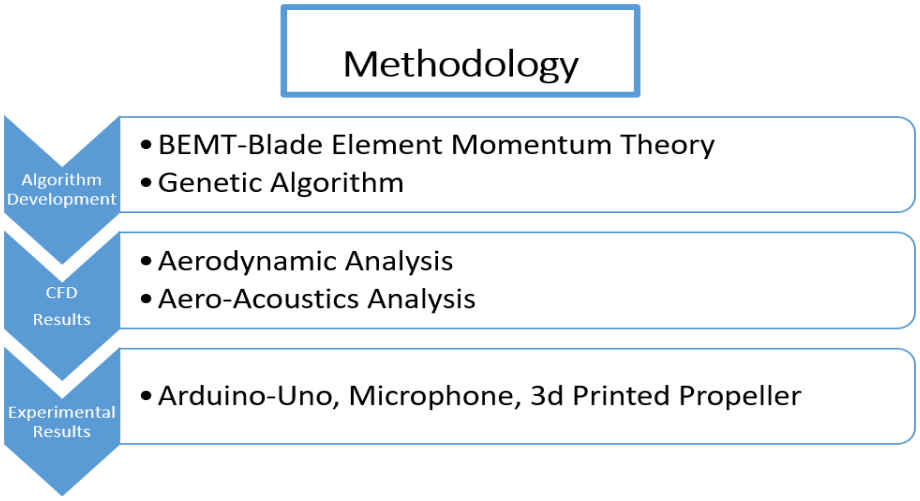

Figure 11: Principle Work-flow of the Thesis Step by Step.

4.1 Algorithm Development

4.1.1 Blade Element Momentum Theory (BEMT) Approach

Blade Element Momentum Theory (BEMT) is widely used for modeling the aerodynamic performance of propellers. In this method, the propeller blade is divided into small sections, and the local aerodynamic forces (lift and drag) at each section are computed. The total thrust and torque generated by the propeller are then obtained by integrating the contributions from each section. For this study, BEMT is applied to analyze the aerodynamic characteristics of an 8-inch diameter UAV propeller with 11 blade sections. The Prandtl's tip loss correction is implemented to account for induced drag at the blade tip. Hover conditions are assumed, meaning free-stream velocity $\mathbf{V}\infty = \mathbf{0}$.

To perform the calculations, the BEMT model is implemented using Python. The following code computes the thrust and torque for a given propeller configuration this implementation provides a baseline aerodynamic performance for the propeller. The full implementation is provided in **Appendix B**.

4.1.2 Genetic Algorithm Optimization with BEMT

A Genetic Algorithm (GA) is employed to optimize chord distribution by maximizing the thrust-to-torque ratio. The GA follows:

I. Set Target Fitness Value (Efficiency)
II. Initial Population (50,000)
III. Fitness Function (BEMT)
IV. Selection (top 80%)
V. Crossover
VI. Mutation
VII. Start over again until reaching target fitness

Here is the flow chart with each step is given below from start to end.

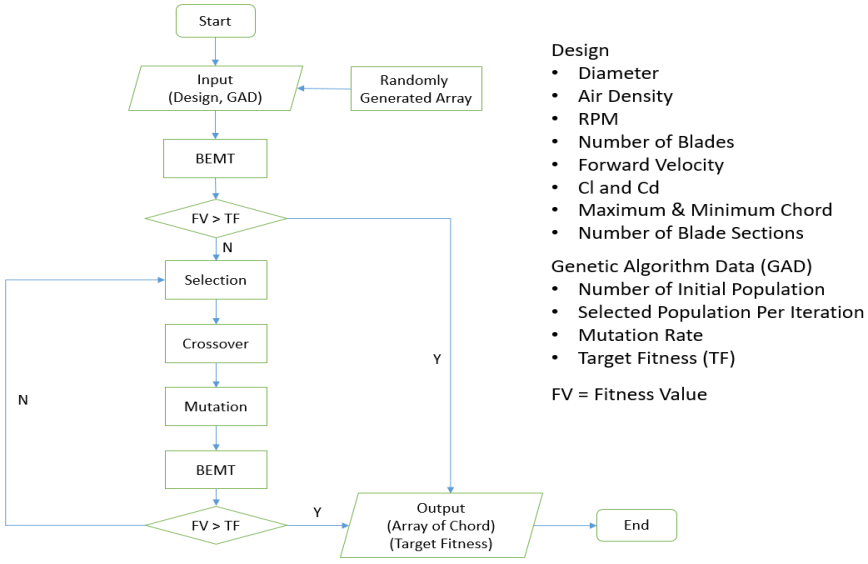

Figure 12: Working Procedure Flowchart of BEMT with Genetic Algorithm

The full implementation is provided in **Appendix B**.

4.1.3 Design Data and Its Optimized Data

APC 8045 Propeller or baseline propeller design data and optimized propeller design are given in this section. Optimized data are found by varying chord length while others parameter are remain constant. By using both data we take further steps. Those are discussed in the different section.

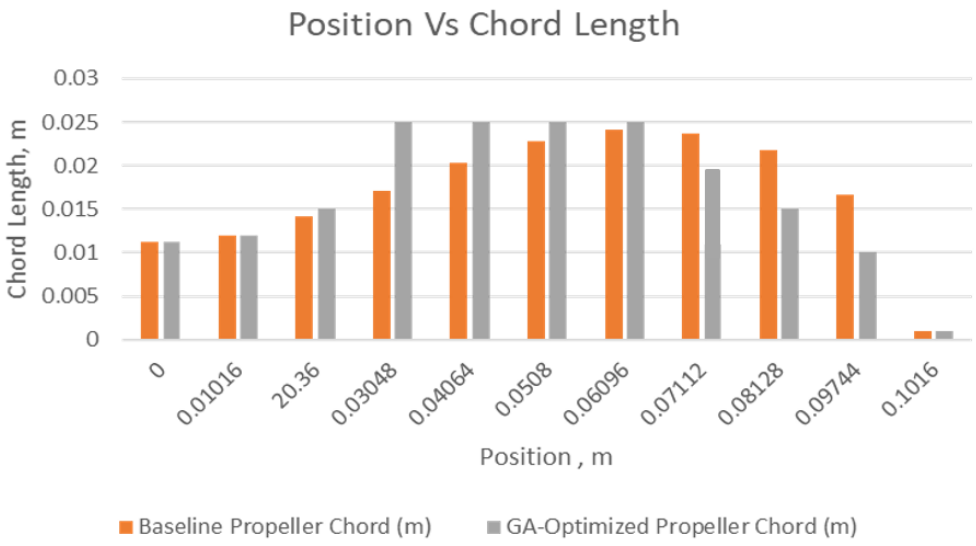

Figure 13: Comparison of Position Vs Chord Length Baseline and GA Optimized Propeller

4.1.4 Fitness Convergence Analysis

To assess the convergence behavior of the Genetic Algorithm (GA) optimization, the fitness values (i.e., thrust-to-torque ratio) were tracked across multiple generations. The objective was to maximize the aerodynamic efficiency of the propeller by evolving optimal chord distributions.

The fitness evolution across 100 generations is visualized in Figure (figure number), which illustrates how the best-performing designs progressively improve. The graph demonstrates rapid improvement in the early generations, followed by gradual convergence as the GA refines the solution.

The fitness function used is defined as:

$$Fitness = \frac{Thrust}{Torque \times \omega} \tag{37}$$

Where Thrust (T) and Torque (Q) are computed from Blade Element Momentum Theory (BEMT), and ω is the rotational velocity.

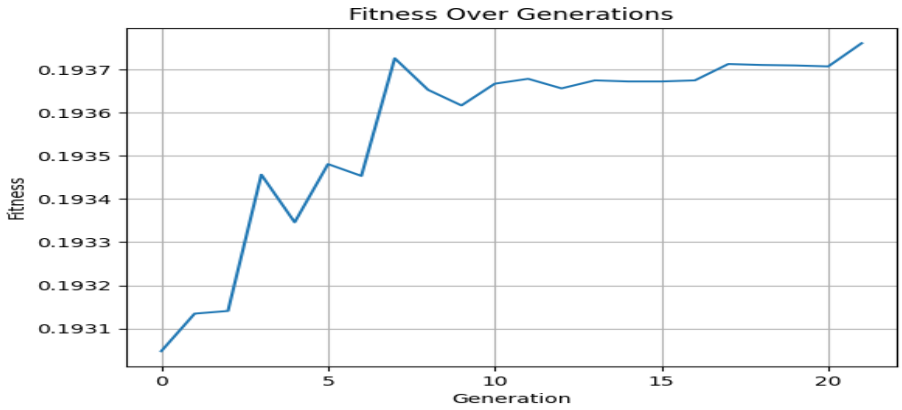

Figure 14 : Evolution of Fitness over Generations in the Genetic Algorithm

4.2 Geometry Generation

After obtaining the optimized chord distribution and blade shape from the Genetic Algorithm (GA) with BEMT, the final propeller geometry was generated in SolidWorks. The design process followed these key steps:

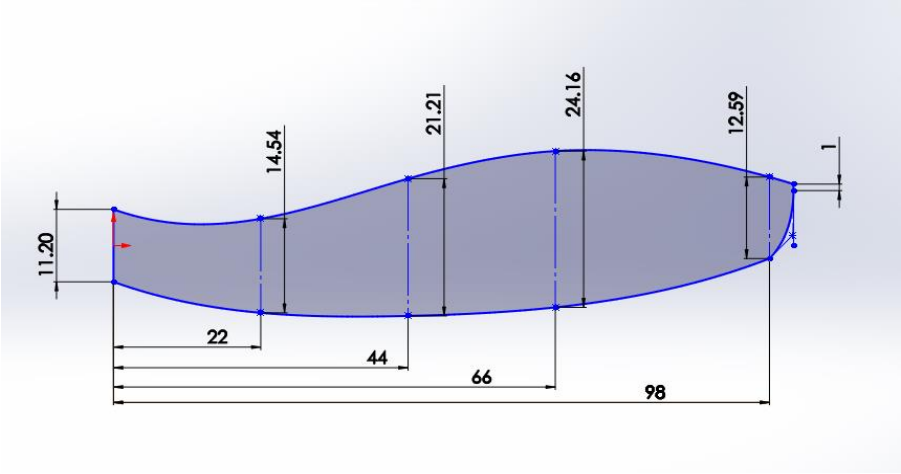

Figure 15: Top View of the Baseline Propeller with Design Data

The optimized chord length distribution obtained from the genetic algorithm (GA) was used to define the blade profile along its span. This ensured that the blade geometry was aerodynamically efficient, leveraging the GA's ability to determine an optimal balance between lift and drag. Additionally, airfoil sections were carefully selected based on aerodynamic efficiency, providing smooth airflow characteristics and minimizing performance losses due to flow separation or turbulence.

Using the optimized parameters, a parametric 3D model of the blade was developed in SolidWorks. The chord, twist, and span values were integrated into the design, allowing for precise control over the aerodynamic shape. A loft feature was applied to incorporate the necessary blade twist, ensuring a smooth aerodynamic transition from the root to the tip. Further modifications were made to the leading-edge and trailing-edge profiles, incorporating serrations and tip area reductions to mitigate noise while maintaining structural integrity and aerodynamic performance.

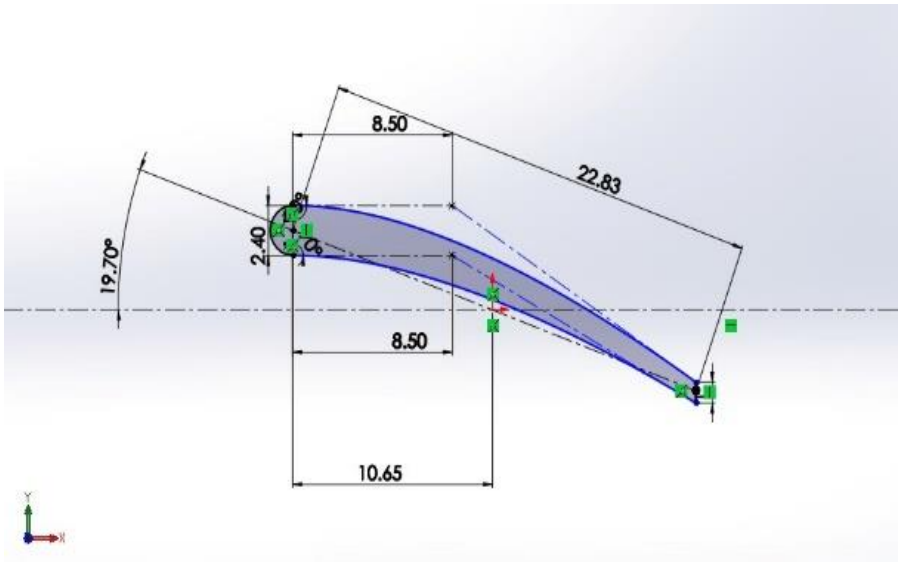

Figure 16: Propeller Airfoil Section at 50.08 mm Radius

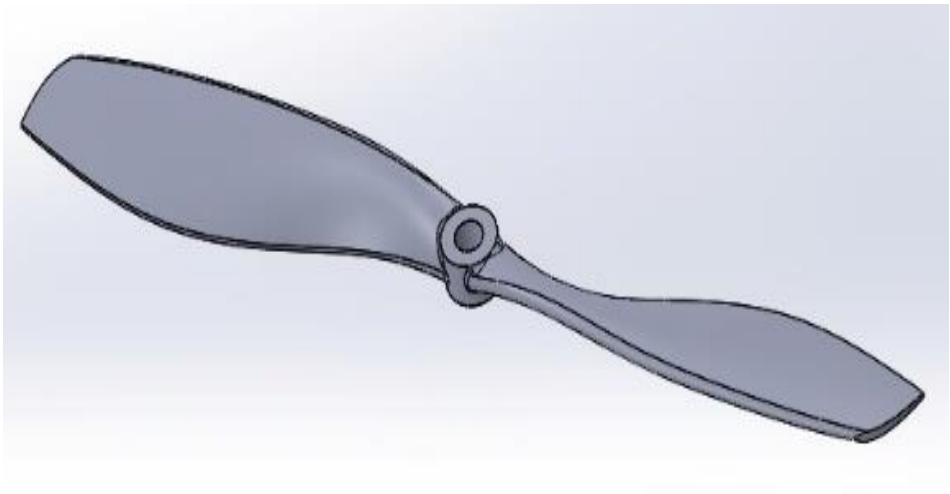

Figure 17: Baseline Propeller CAD View

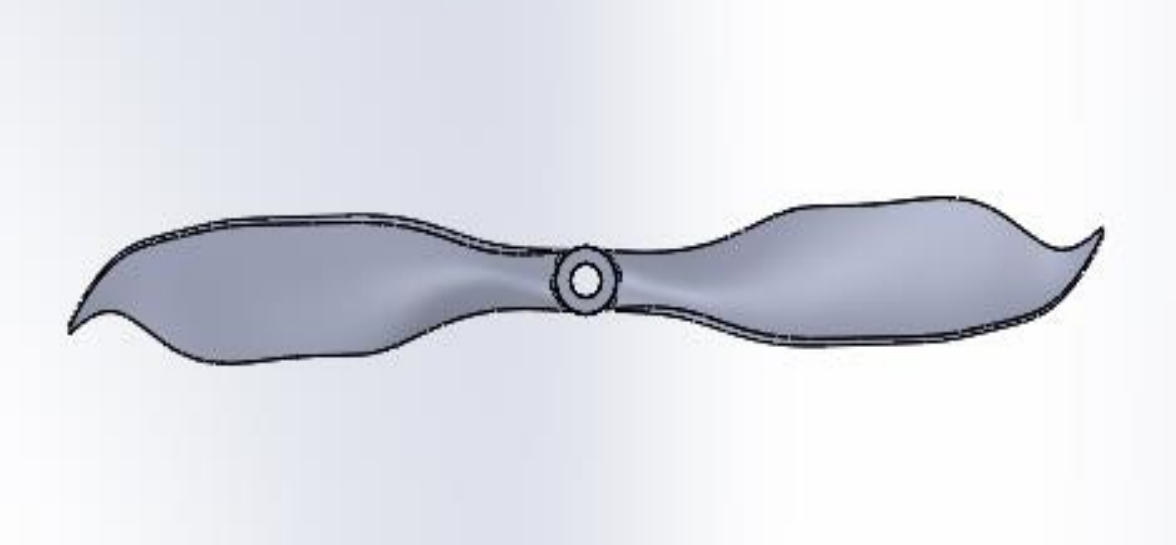

Figure 18: GA Optimized Propeller CAD View

Once the final design was completed, the SolidWorks model was exported in STL and STEP formats to facilitate both computational fluid dynamics (CFD) simulations and manufacturing processes. Before conducting simulations, a high-resolution mesh refinement study was performed to ensure numerical accuracy and stability. The exported files also enabled rapid prototyping through 3D printing, allowing for physical validation of the design in experimental setup tests.

4.3 Computational Fluid Dynamics (CFD) Simulation

To evaluate the aerodynamic and acoustic performance of the optimized propeller, CFD simulations were performed in ANSYS Fluent. The simulation workflow was as follows:

4.3.1 Aerodynamic Analysis

Solver Approach: Steady-state Reynolds-Averaged Navier-Stokes (RANS) equations were used with different turbulence models and grid cell size.

4.3.1.1 Grid Independence Test

For ensuring grid independence and minimize computational errors, three different computational domains were tested during the simulation process. The domain cell size, measuring 0.42 million, 0.73 million and 0.96 million was tested to calculate thrust, torque and y+ value. Comparing these domains we take 0.42 million to do further simulation that provided reliable simulation accuracy without excessive computational overhead as all the cell size give almost the same value.

Table 1: Thrust, Torque, y+ in Different RPM for Grid Independence Test of Different Cell

Cell No (million)	RPM	Thrust(N)	Torque	y+
0.42	3000	0.6403	0.0119	0.2164
0.42	4000	1.1175	0.0213	0.3206
0.42	5000	1.7497	0.0333	0.3914
0.73	3000	0.6216	0.0115	0.2988
0.73	4000	1.1169	0.0205	0.3834
0.73	5000	1.7567	0.0319	0.4651
0.96	3000	0.6188	0.0113	0.3241
0.96	4000	1.1144	0.0202	0.4139
0.96	5000	1.7531	0.0314	0.5018

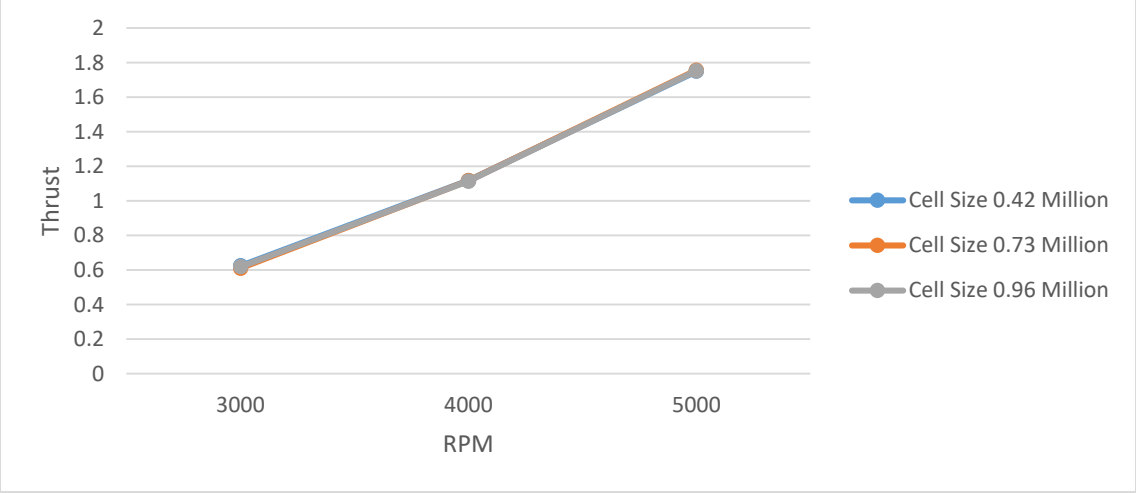

Figure 19: Thrust Vs RPM for Grid Independence Test of Different Cell

4.3.1.2 Turbulence Model Selection

Three turbulence model are used to perform simulation:

- **Shear Stress Transport (SST) k-ω**
- **Realizable k-ε**
- **Spalart-Allmaras (SA)**

Table 2: Different Turbulence Model Comparison with Thrust, Torque and y+

Model	Cell No (million)	RPM	Thrust (N)	Torque (Nm)	y+
SST k-w	0.42	3000	0.6403	0.0113	0.2164
Realiazable k-e	0.42	3000	0.6384	0.0116	0.2164
SA	0.42	3000	0.6444	0.0119	0.2164
SST k-w	0.42	4000	1.1381	0.0202	0.2764
Realiazable k-e	0.42	4000	1.1258	0.0205	0.3107
SA	0.42	4000	1.1375	0.0213	0.3206
SST k-w	0.42	5000	1.7707	0.0314	0.3346
Realiazable k-e	0.42	5000	1.7636	0.0319	0.3741
SA	0.42	5000	1.7797	0.0333	0.3914

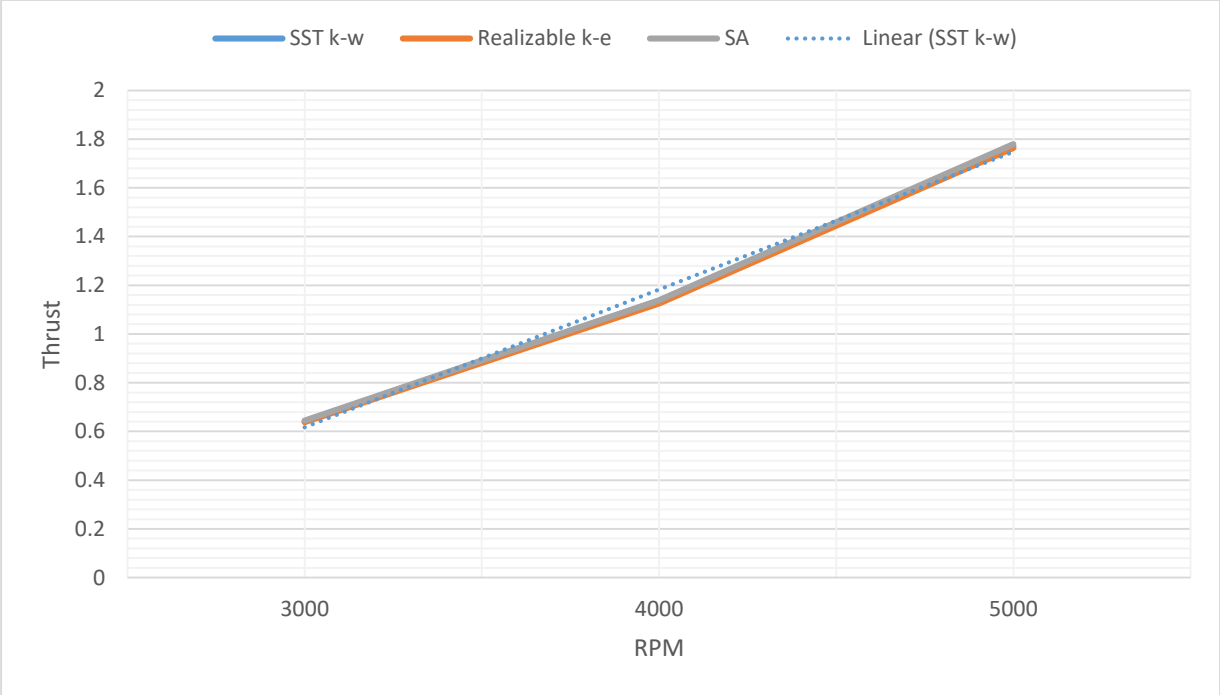

Figure 20: Thrust Vs RPM for Different Turbulence Model

From the Table and graph, it shows SST k-w give value somewhat is almost the mean in between all three of the turbulence model. So that we select SST k-w for further simulation.

4.3.1.3 CFD Model Setup and Final Processing

To ensure the accuracy of the simulation, carefully chosen boundary conditions were applied. The airflow entering the domain was set as a velocity inlet, replicating real-world free-stream conditions, while the outlet maintained atmospheric pressure for a natural flow exit. A no-slip condition was applied to the propeller surfaces, meaning air couldn't slip past the blades, allowing for a realistic representation of aerodynamic forces. Since the propeller spins at high speeds, a Moving Reference Frame (MRF) approach was used to model its rotation at 3000, 4000, and 5000 RPM along the Y-axis, making the simulation both efficient and reliable.

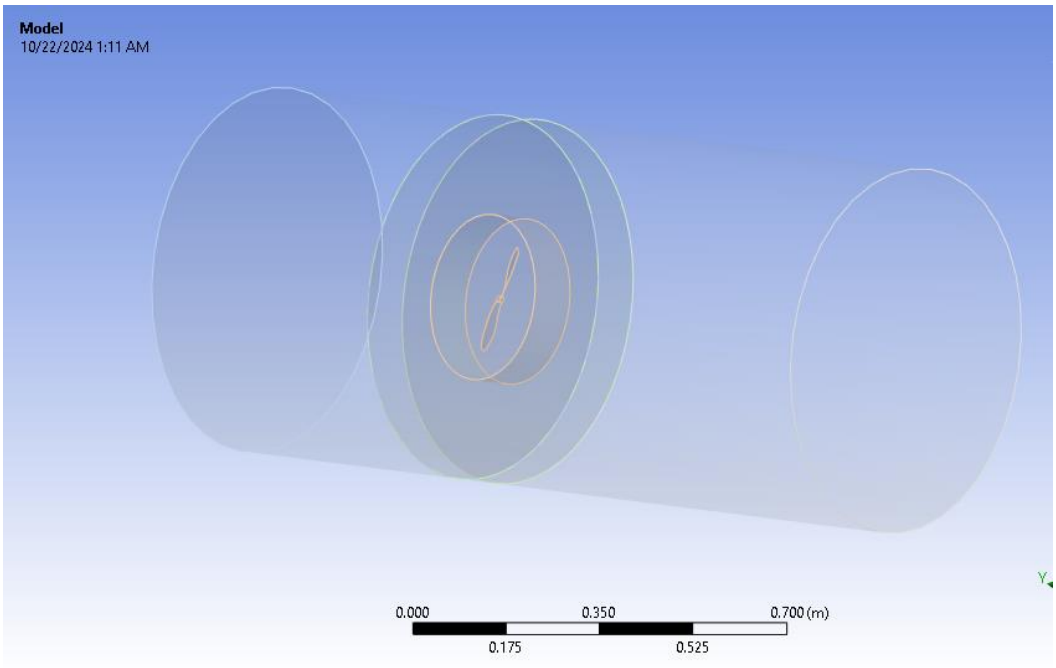

Figure 21: Simulation Model

Creating a high-quality mesh was crucial to capturing the intricate airflow details. A fine, unstructured tetrahedral mesh was generated, ensuring that the propeller's surface was well-defined. To improve accuracy, inflation layers were added near the propeller blades, helping to better resolve the boundary layer where most aerodynamic forces occur. Mesh Skewness was maximum 0.89, where, <1 is permitted and it implies that the mesh is ready for calculation. One of the key aspects of maintaining precision was keeping the average y-plus value between 0.2 and 0.4, which ensured the simulation could accurately capture the near-wall airflow behavior without excessive computational cost.

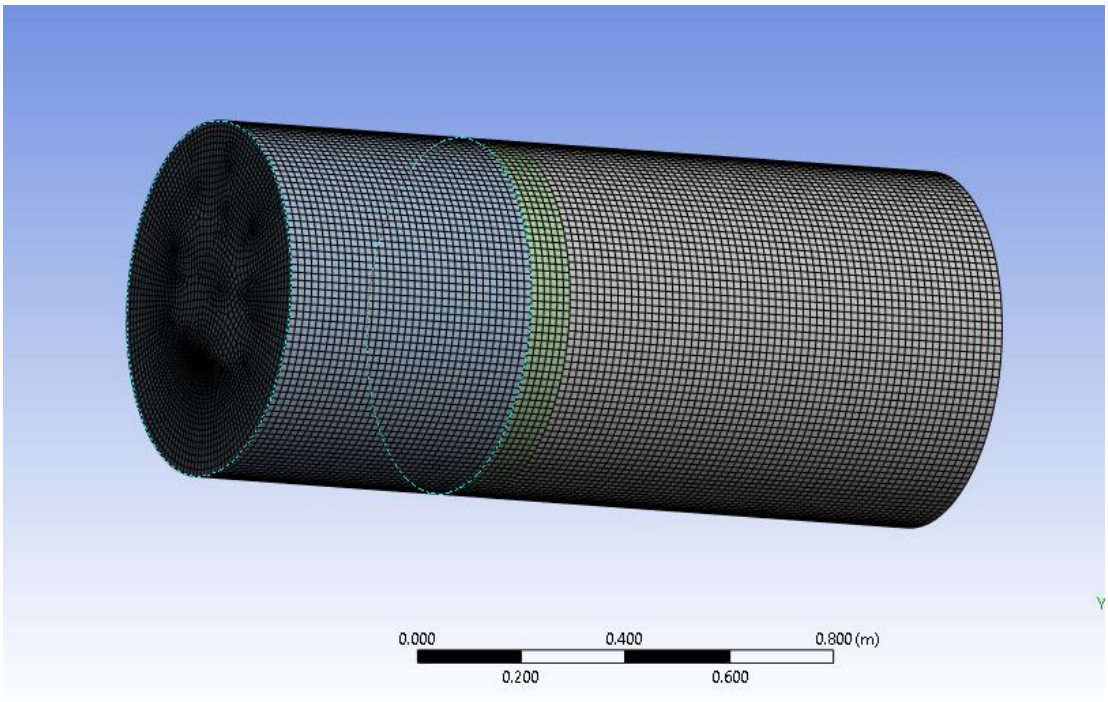

Figure 22: Mesh of the Model

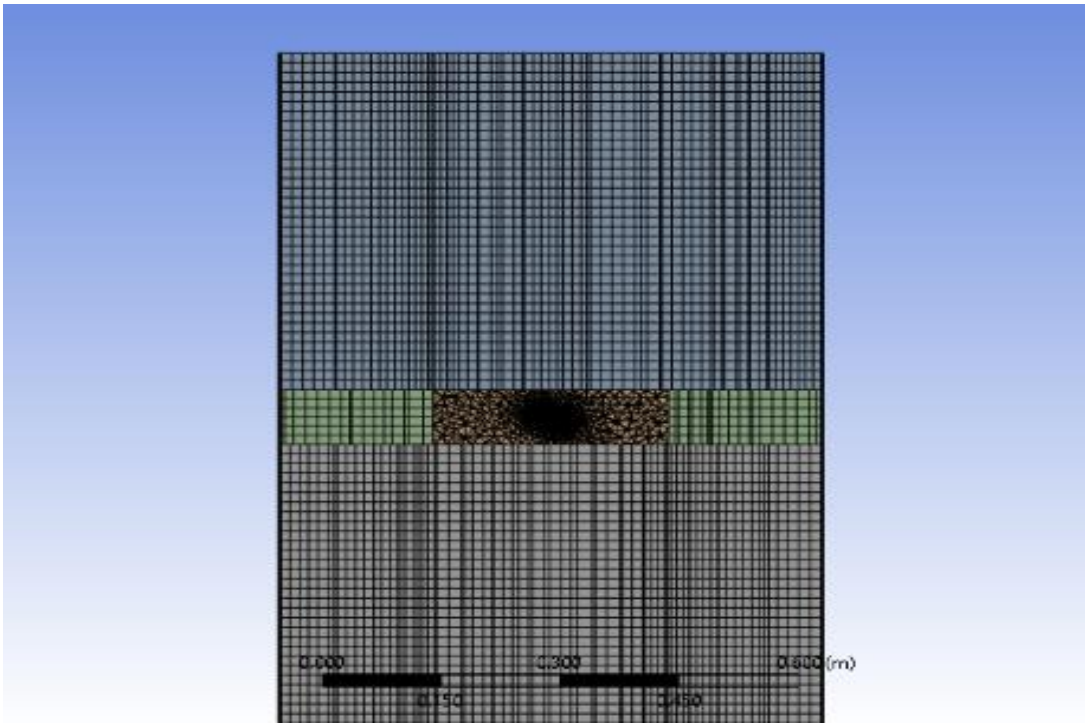

Figure 23: Mesh Around the Blade

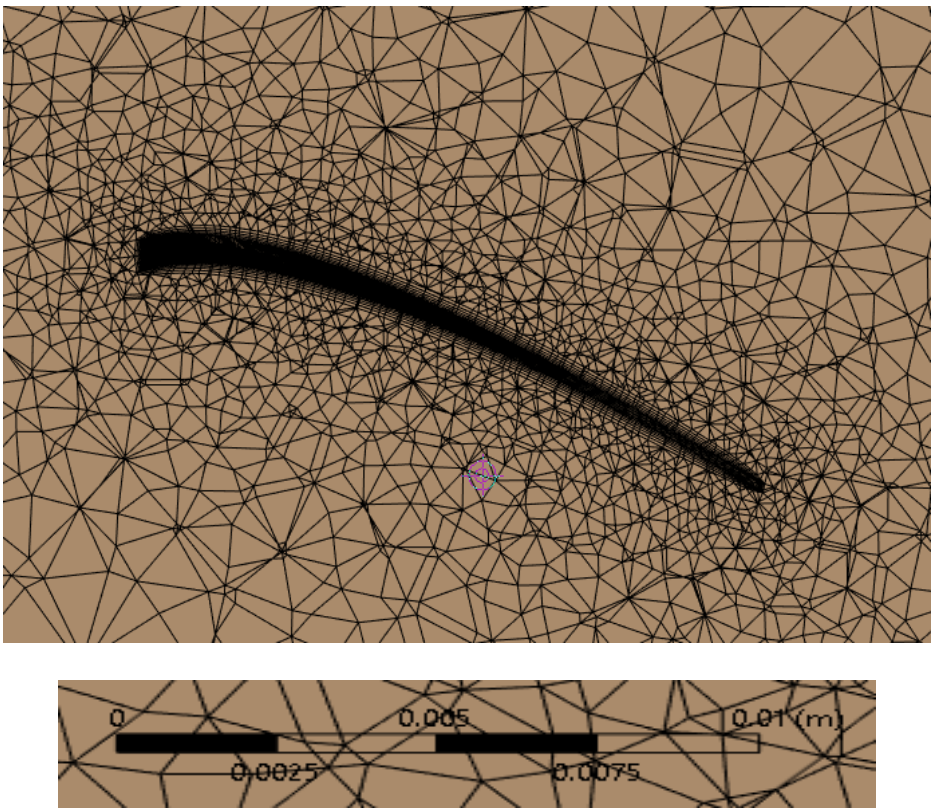

Figure 24: Inflation Layer Around the Blade

Table 3: Mesh Metric of Skewness

Mesh Metric	Skewness
Min	1.13e-005
Max	0.88985
Average	0.20894
Standard Deviation	0.14438

Once everything was set up, the simulation was run to calculate key performance metrics, such as thrust and torque. These values were then compared with experimental results to validate the accuracy of the model. By ensuring the simulation closely matched real-world data, it became a reliable tool for analyzing and optimizing the propeller's design. This validation step was essential in confirming that the results could be used confidently for further refinement and practical applications.

4.3.2 Aeroacoustic Analysis

Understanding how the propeller generates noise required a detailed CFD simulation using advanced turbulence models like Detached Eddy Simulation (DES) and Large Eddy Simulation (LES). These models helped capture the complex airflow patterns responsible for noise. To realistically simulate the propeller's spinning motion and its interaction with air, a sliding mesh technique was used, allowing the simulation to reflect real-world conditions more accurately.

The solver settings were carefully adjusted to ensure accurate results. The PISO scheme was applied for stable airflow calculations, while key acoustic outputs were measured. These included tonal noise caused by the blade passing frequency (BPF), broadband noise from turbulence, and the overall sound pressure level (SPL) in decibels. Analyzing these factors provided valuable insights into how different propeller designs affected noise levels and aerodynamic efficiency.

Once the simulation was completed, Fast Fourier Transform (FFT) analysis helped break down the noise data and identify dominant sound sources. This made it easier to determine which aspects of the design contributed most to noise and whether modifications like serrations and tip adjustments were effective in reducing it. The results provided a clearer picture of the optimized propeller's performance, guiding improvements for quieter and more efficient designs.

4.4 Experimental Setup for Propeller Testing

4.4.1 3D Printing and Manufacturing

After successfully validating the optimized propeller design through CFD simulations, the next step was to bring the design to life using 3D printing. Choosing the right material was essential to balance durability and performance. PLA+ filament was selected because it is both lightweight and strong, making it ideal for aerodynamic applications. To achieve a smooth surface finish and reduce roughness, SLA printing was also used, ensuring better airflow over the blades.

Creatility software and printer was used to print those design. Solid works design file firstly imported as STL file into a computer where creatility software are installed, after then then open source software process the file further to make it fit for 3d printing. After modification the file, it directly send to the 3d print to print it layer by layer. A schematic diagram and some steps of 3d printing are given below-

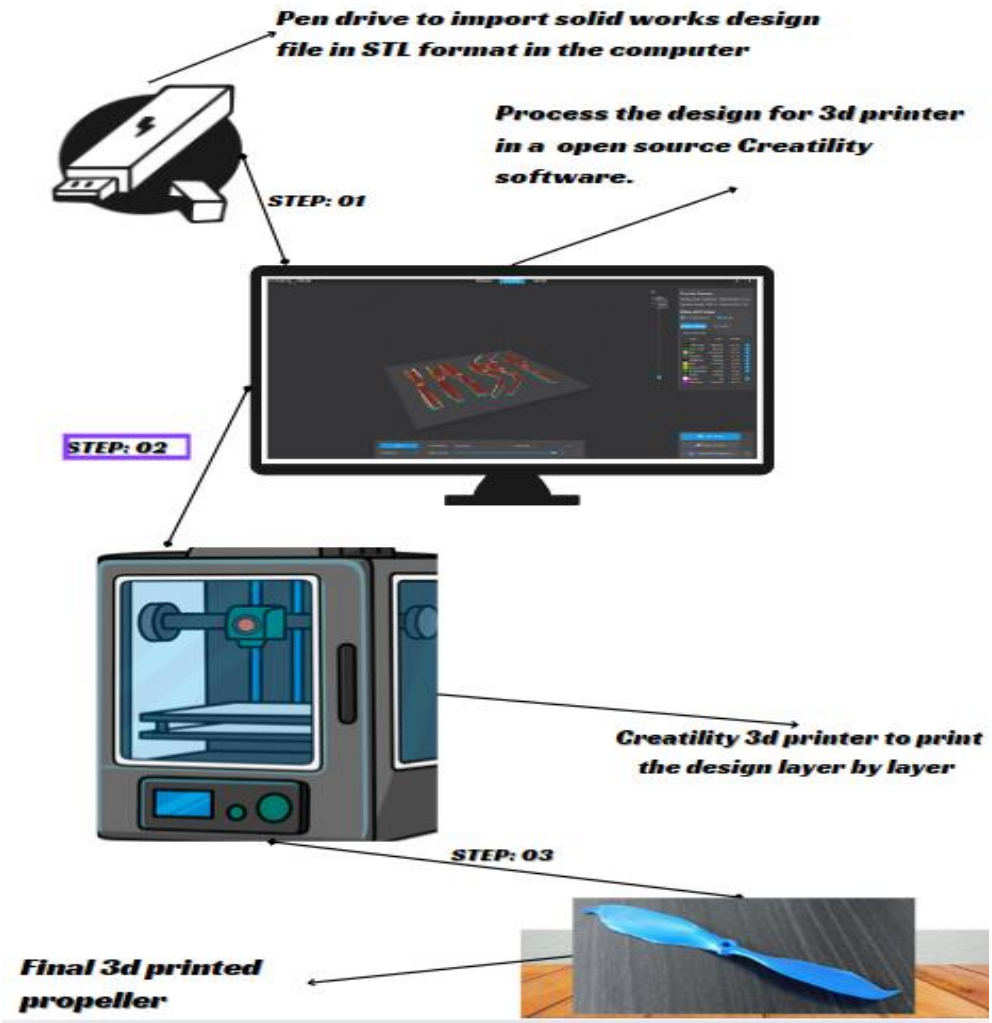

Figure 25: Schematic Diagram of 3D Printing Process

Figure 26: 3D printed Baseline Propeller

Figure 27: 3D Printed Optimized Propeller Top view

The printing process involved creating two types of propellers: one baseline design without modifications and another with the optimized features, including tip adjustments. This side-by-side approach allowed for a direct performance comparison between the standard and improved designs. Once printed, the propellers went through careful post-processing, including sanding and polishing, to eliminate surface imperfections. This final touch ensured that the blades were as smooth and aerodynamic as possible, preparing them for real-world testing and performance evaluation.

4.4.2 Test Setup Fabrication

The experimental setup was designed to evaluate both aerodynamic and aeroacoustic performance, ensuring a comprehensive assessment of the 3D-printed propellers. A BLDC motor was used to drive the propellers at various RPM levels, while a load cell with an amplifier accurately measured the thrust force generated. To monitor rotational speed, an IR sensor captured real-time RPM data, which was processed using an Arduino Uno as the central controller. Torque estimation was performed using a multimeter, measuring the motor's current draw to assess power consumption and efficiency.

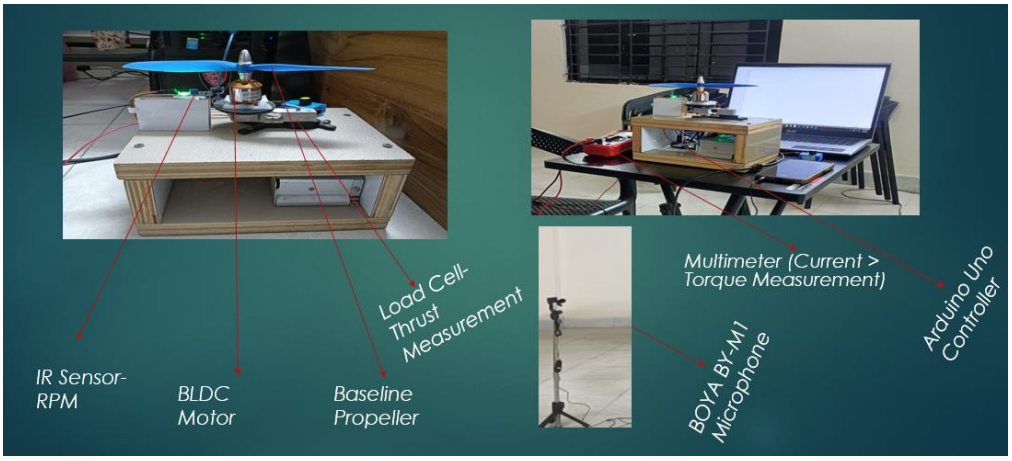

Figure 28: Diagram of the Experimental Setup

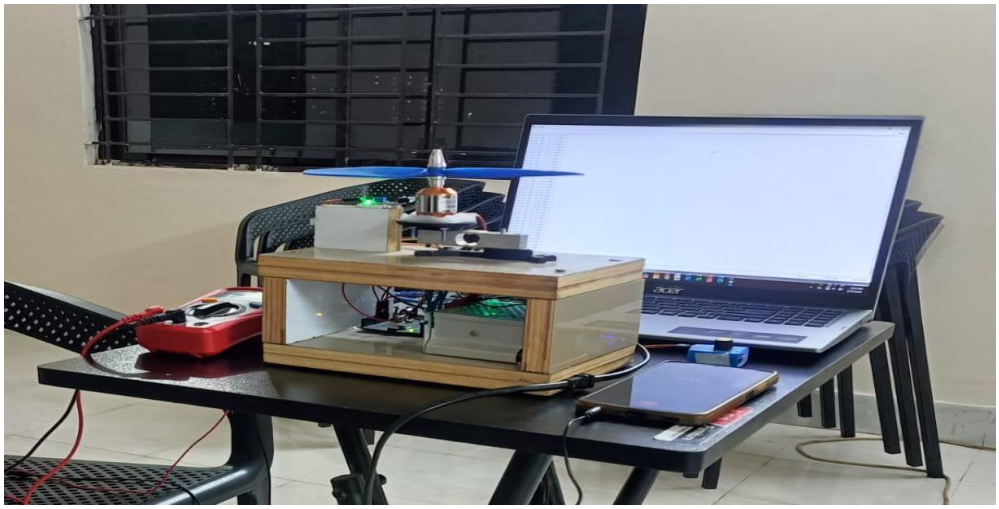

Figure 29: Aerodynamic Thrust and Torque Measurement Setup

For aeroacoustic validation, a noise measurement system was integrated into the setup. A high-sensitivity BOYA BY-M1 microphone was placed 1.5 meters away from the propeller to record sound data while minimizing environmental interference. Background noise levels were carefully accounted for to ensure accurate readings. The recorded noise signals were then analyzed in MATLAB using Fast Fourier Transform (FFT), allowing for the identification of tonal noise at the blade passing frequency (BPF) and broadband noise generated by turbulence.

Figure 30: Aeroacoustic Sound Measurement Setup using Boya BY-MI

The noise reduction effectiveness of the optimized propeller designs was evaluated by comparing the baseline APT 8045 propeller against modified versions featuring tip adjustments. Changes in overall noise levels (dB) and spectral characteristics were closely examined to determine the impact of these modifications. This thorough approach ensured a clear understanding of the aerodynamic efficiency and noise reduction capabilities of the newly designed propellers.

4.4.3 Sensor Validation

To ensure the accuracy and reliability of the experimental setup, the IR sensor (for RPM measurement) and load cell (for thrust measurement) were validated using a tachometer and known weights, respectively.

Load Cell and IR sensor Calibration:

The load cell was calibrated using known weights. By convert the sensor's output into thrust force, the load cell showed an accuracy of ±1.07% across the measurement range, with a repeatability standard deviation of <0.5%. For IR sensor comparing with tachometer it is ±2.33% with a repeatability standard deviation of <1.45%.

Table 4: Load Cell Calibration Table

Known Weight (g)	Measured Weight (g)	True Thrust (N)	Measured Thrust (N)	Error (%)
10.32	10.43	0.1010	0.1020	+0.99%
50.67	51.28	0.4965	0.5027	+1.24%
99.73	100.94	0.9787	0.9892	+1.07%

Table 5: IR Sensor Calibration Table

RPM (IR Sensor)	Measured RPM (Tachometer)	Error (%)
3000	3047	+1.57%
4000	4093	+2.33%
5000	5159	+3.18%

The calibration confirmed that both sensors meet the required accuracy standards. The load cell and IR sensor delivered reliable thrust readings, ensuring the experimental data's reliability for validating computational models.

4.5 Model Validation:

To validate the accuracy of the computational models, the simulation results for thrust and torque were compared with data from a published study [30]. The validation was performed at three RPM levels (3000 RPM, 4000 RPM, and 5000 RPM), and the results are summarized in Table 6.

Table 6: Comparison of Simulation Results with Published Data

	Thrust		Torque	
RPM	Simulation	Paper	Simulation	Paper
3000	0.640273	0.592	0.01137	0.01
4000	1.137691	1.037	0.020119	0.02
5000	1.770715	1.81	0.031237	0.029

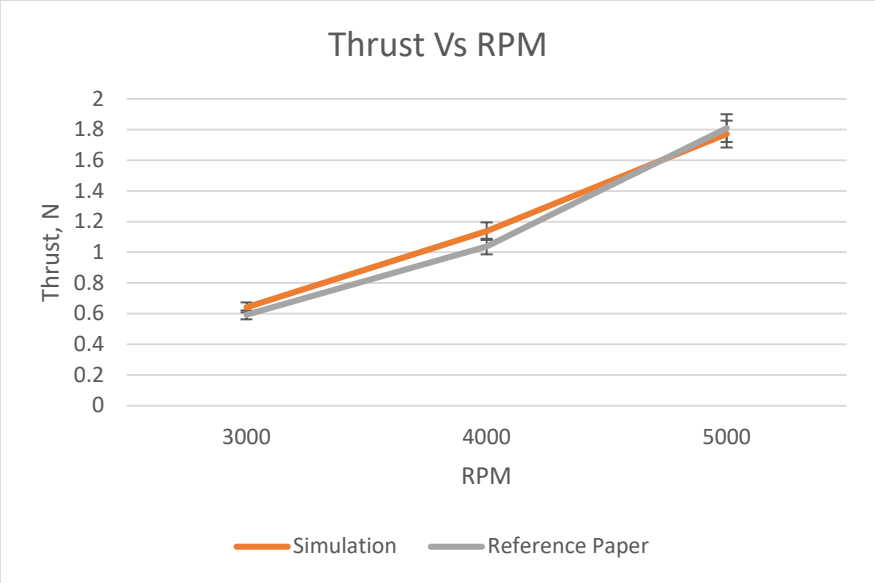

Figure 31: Thrust Comparison between Simulated and Published Data

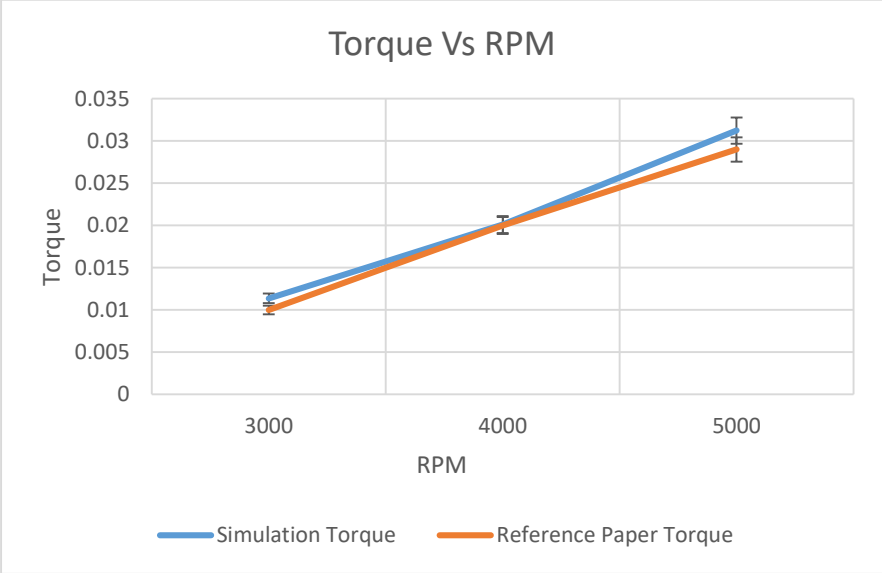

Figure 32: Torque Comparison between Simulated and Published data

The validation study shows all the value is on tolerance level and confirms that the computational model accurately predicts thrust and torque across the tested RPM range when compared to published data. While minor discrepancies exist, particularly at lower RPM, the overall agreement is strong. These results validate the use of the computational model for further analysis and optimization of UAV propellers.

To Validated Our BEMT and Experimental Model we make Comparison these data with simulated data. The Graphs are given below on figure 33 and 34.

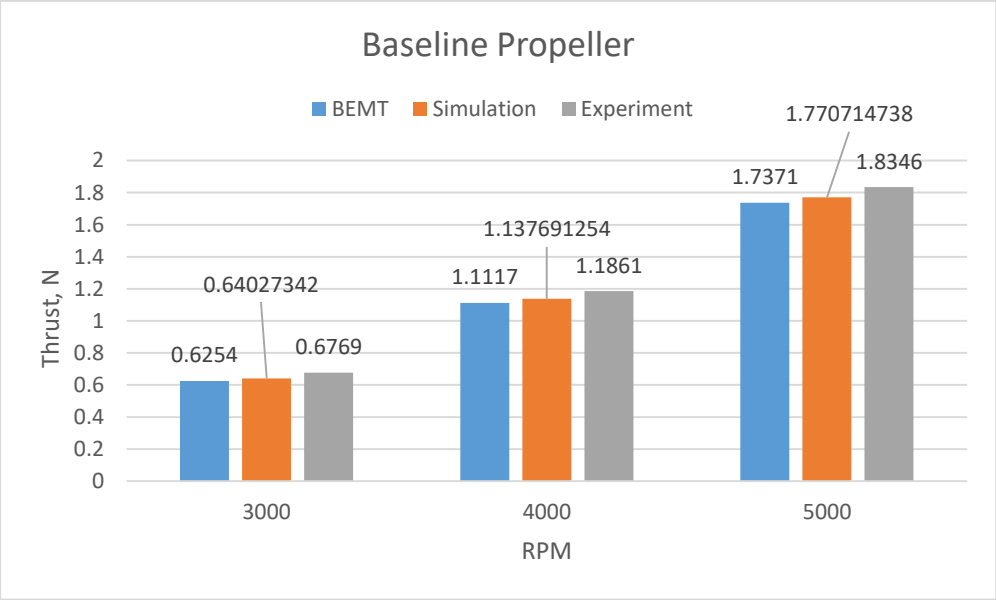

Figure 33: Thrust Comparison between BEMT, Simulated Data and Experimental Data

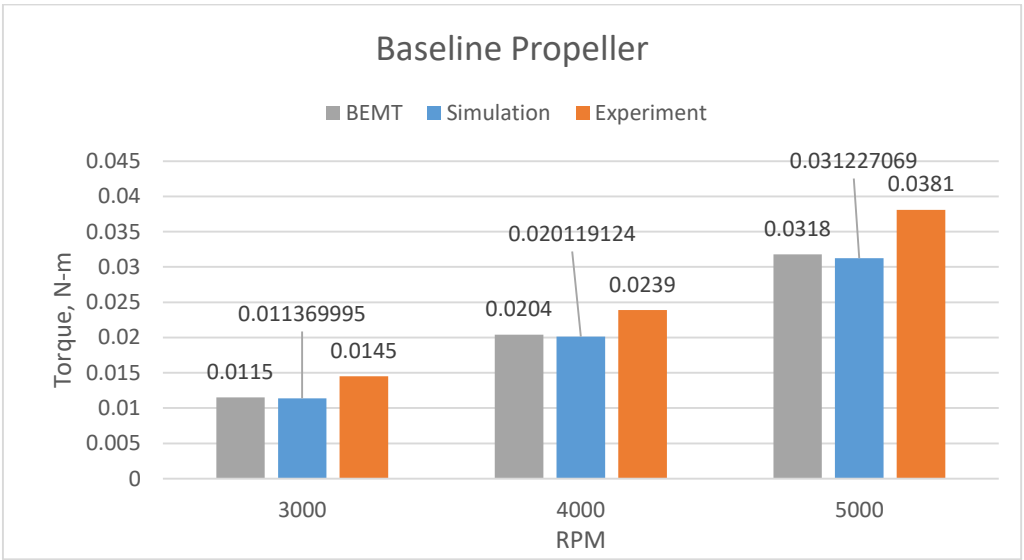

Figure 34: Torque Comparison between BEMT, Simulated Data and Experimental Data

These value shows there is less of uncertainty on experimental test and the BEMT value is almost same as simulated data. So BEMT model as well as are validated and it also indicate the experimental data is also reliable.

Chapter 5: Result and Discussion

This chapter presents the aerodynamic and aeroacoustic performance results of the UAV propeller obtained from CFD simulations and experimental validation. The results are analyzed in terms of thrust, torque, efficiency, and noise characteristics, comparing the baseline propeller with the tip-modified designs.

5.1 Aerodynamic Performance Analysis

5.1.1 Thrust and Torque Comparison

To evaluate the aerodynamic performance of the propeller, we analyzed its thrust and torque characteristics using BEMT calculations**,** CFD simulations and Experiment. The comparison focuses on how the baseline propeller performs against the Genetic Algorithm (GA)-optimized design across different rotational speeds.

Thrust Analysis:

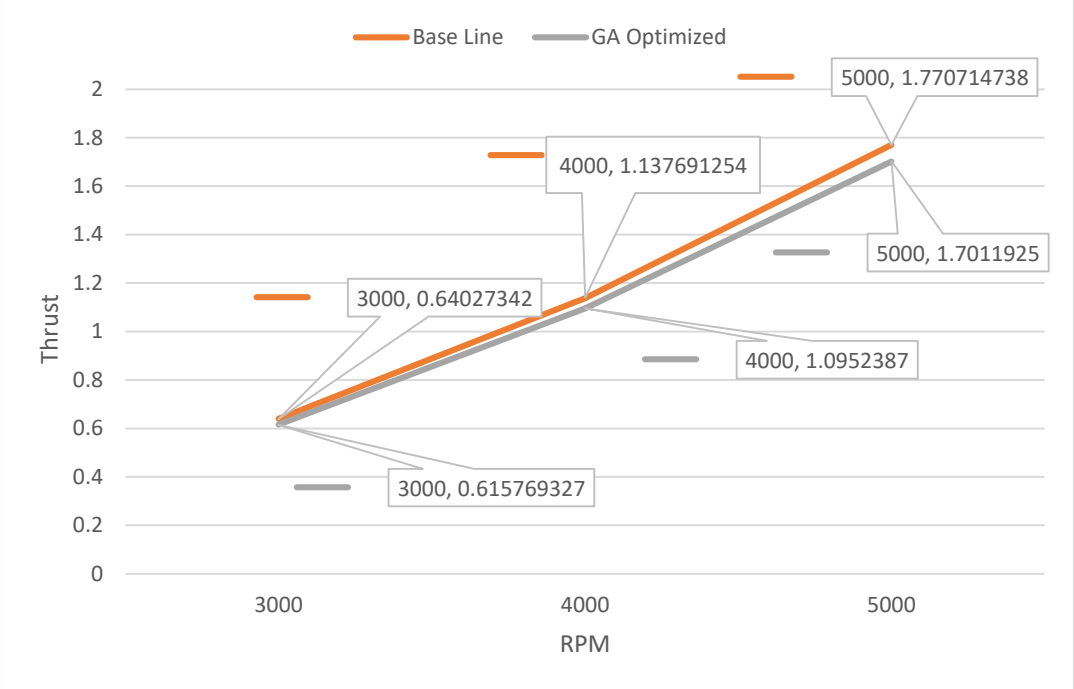

Figure 35: CFD - Thrust Vs RPM for Baseline and GA Optimized Propeller

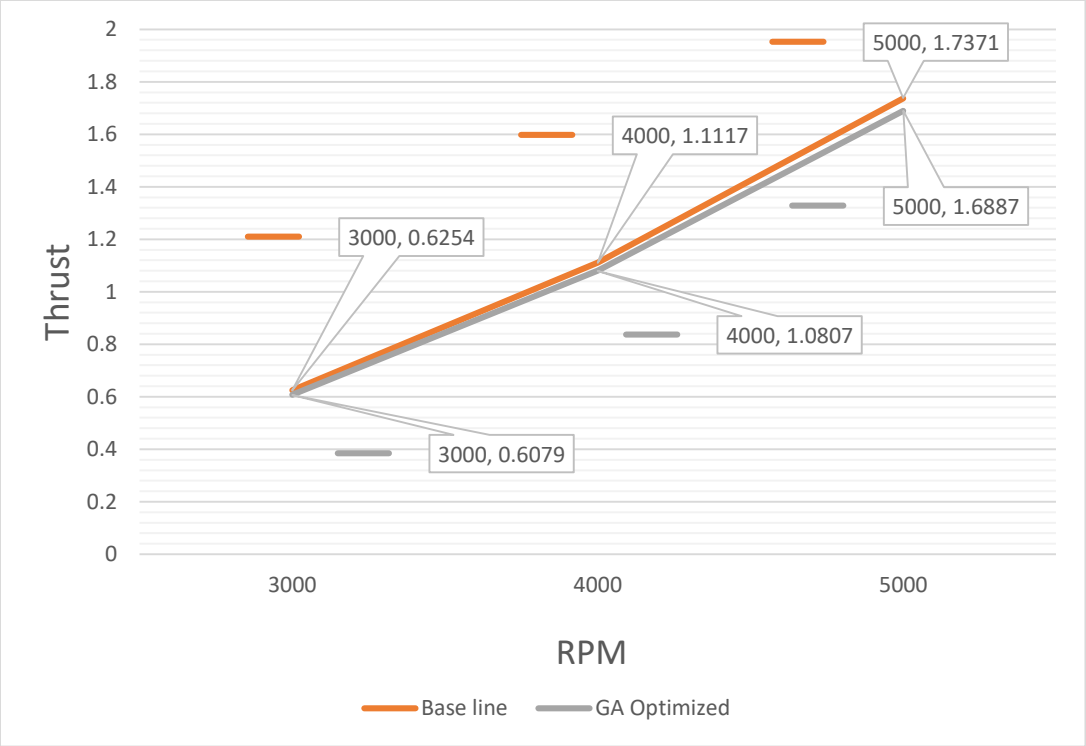

Figure 36: BEMT - Thrust Vs RPM for Baseline and GA Optimized Propeller

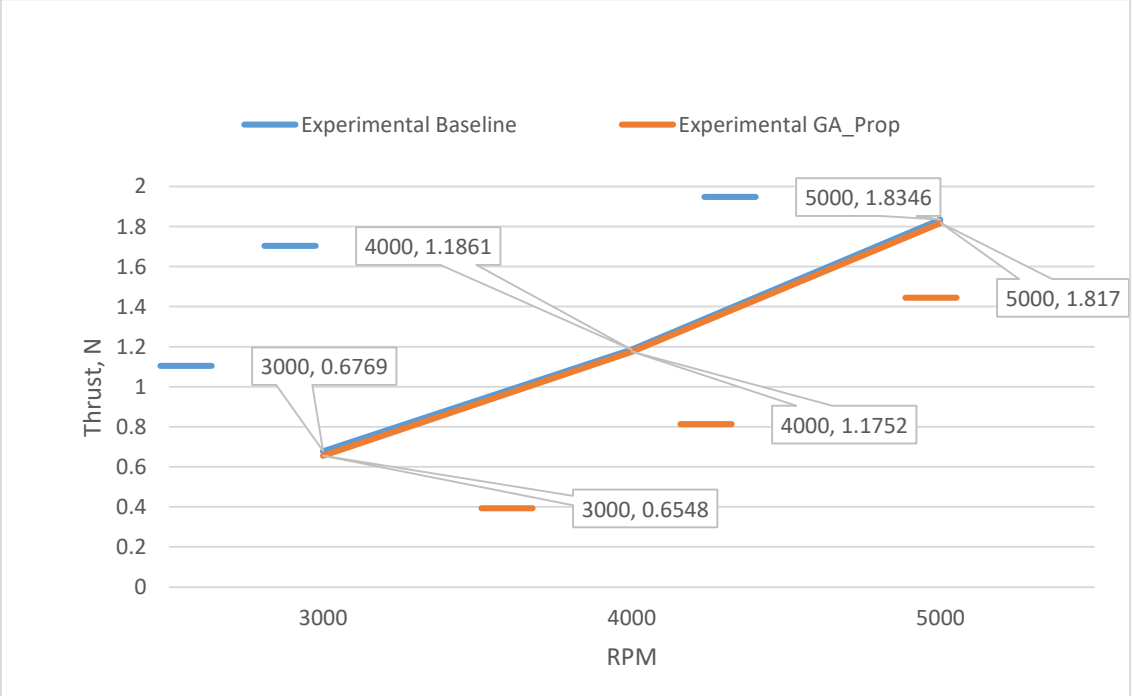

Figure 37: Experimental - Thrust Vs RPM for Baseline and GA Optimized Propeller

The simulated thrust values show that the GA-optimized propeller consistently produces slightly lower thrust compared to the baseline across all RPM levels. At 3000 RPM, the thrust is reduced from 0.640 N to 0.616 N, and at 5000 RPM, it decreases from 1.771 N to 1.701 N. A similar trend is observed in the Experimental and BEMT-based thrust predictions, where the GA-optimized propeller exhibits a marginal reduction in thrust output.

This reduction suggests that the optimization process prioritized efficiency over absolute thrust production. The observed changes may be attributed to modifications in blade geometry, particularly at the tip region, which could have altered the lift distribution and vortex dynamics.

Torque Analysis:

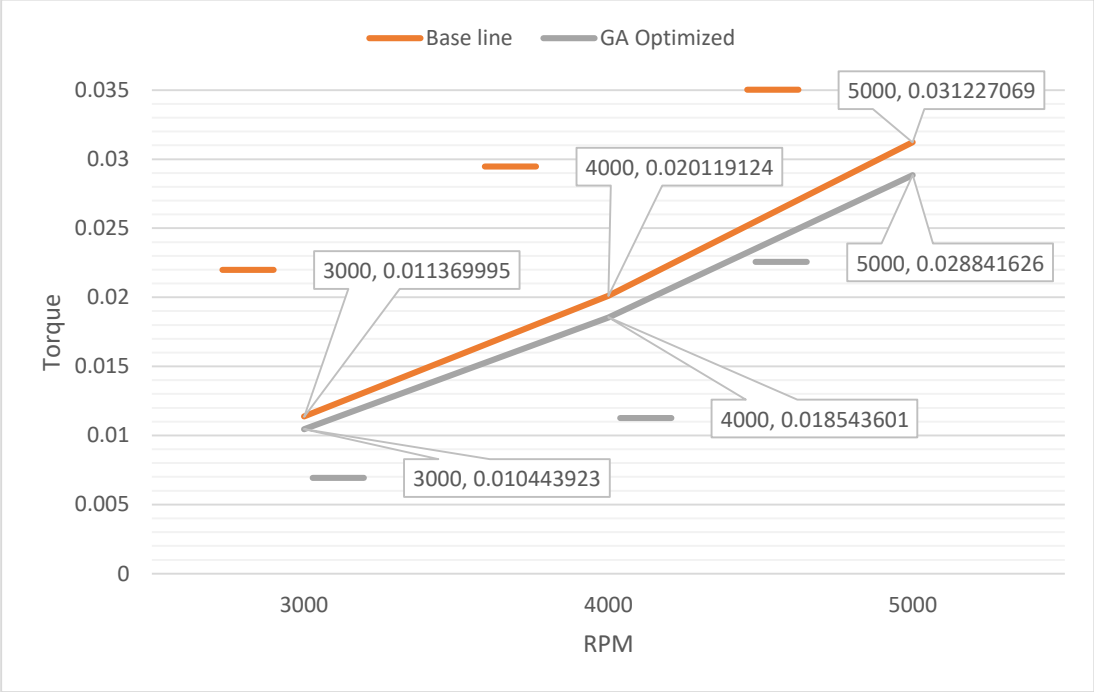

Figure 38: CFD - Torque Vs RPM for Baseline and GA Optimized Propeller

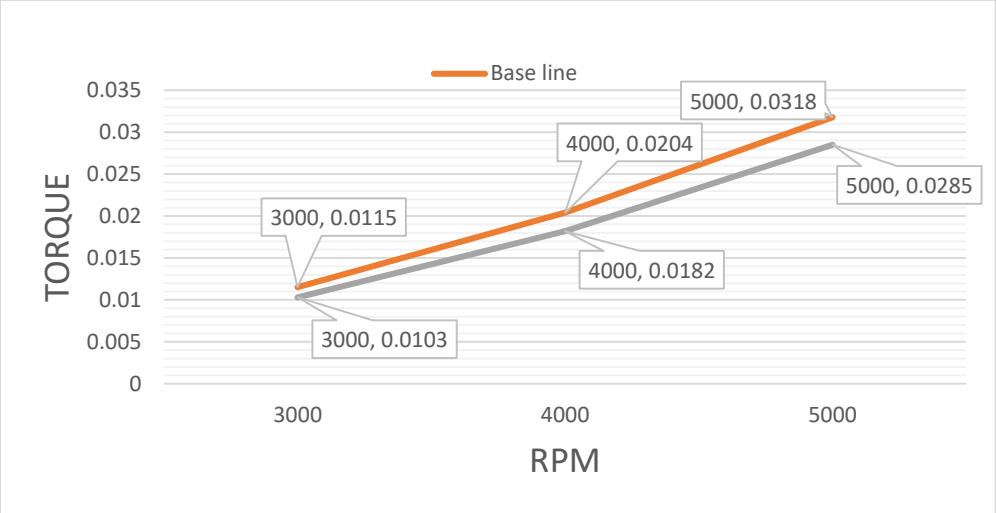

Figure 39: BEMT - Torque Vs RPM for Baseline and GA Optimized Propeller

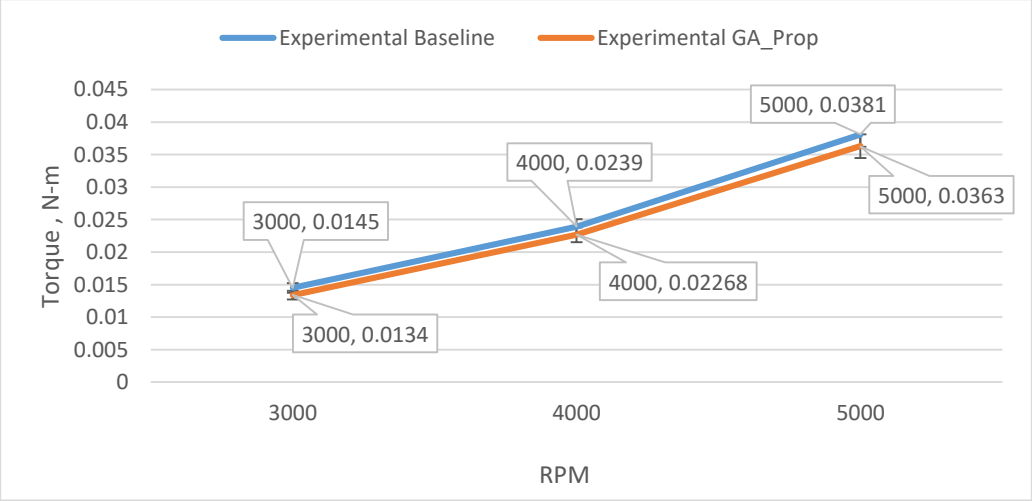

Figure 40: Experimental -Torque Vs RPM for Baseline and GA Optimized Propeller

Torque values, both three from simulations, Experiment and BEMT calculations, indicate a noticeable reduction for the GA-optimized propeller. For instance, at 3000 RPM, the simulated torque decreases from 0.01137 Nm (baseline) to 0.01044 Nm (optimized). Similarly, at 5000 RPM, the torque drops from 0.03123 Nm to 0.02884 Nm. The Experimental and BEMT-derived torque values follow the same trend, reinforcing the reliability of the computational analysis.

The reduced torque requirements suggest that the optimized propeller design improves aerodynamic efficiency, requiring less input power to generate comparable thrust levels. This

efficiency gain could be beneficial for UAV applications where power consumption directly impacts flight endurance.

5.1.2 Efficiency and Power Consumption

Thrust-to-Power Ratio Comparison

The thrust-to-power ratio (η) is a critical parameter for evaluating propeller performance, as it measures how efficiently the propeller converts input power into thrust. A higher ratio signifies improved aerodynamic efficiency, meaning the propeller generates more thrust while consuming less power. The GA-optimized propeller exhibits a consistent improvement in efficiency across all tested RPM values, with efficiency gains ranging from 4.02% to 4.70% compared to the baseline design.

Table 7: Simulated Efficiency Comparison between Baseline and GA-Optimized Propeller

RPM	Baseline Efficiency	Optimized Efficiency	Improvement (%)
3000	0.1792	0.1877	4.70
4000	0.1350	0.1410	4.45
5000	0.1083	0.1127	4.02

A graph is given below for make it visual.

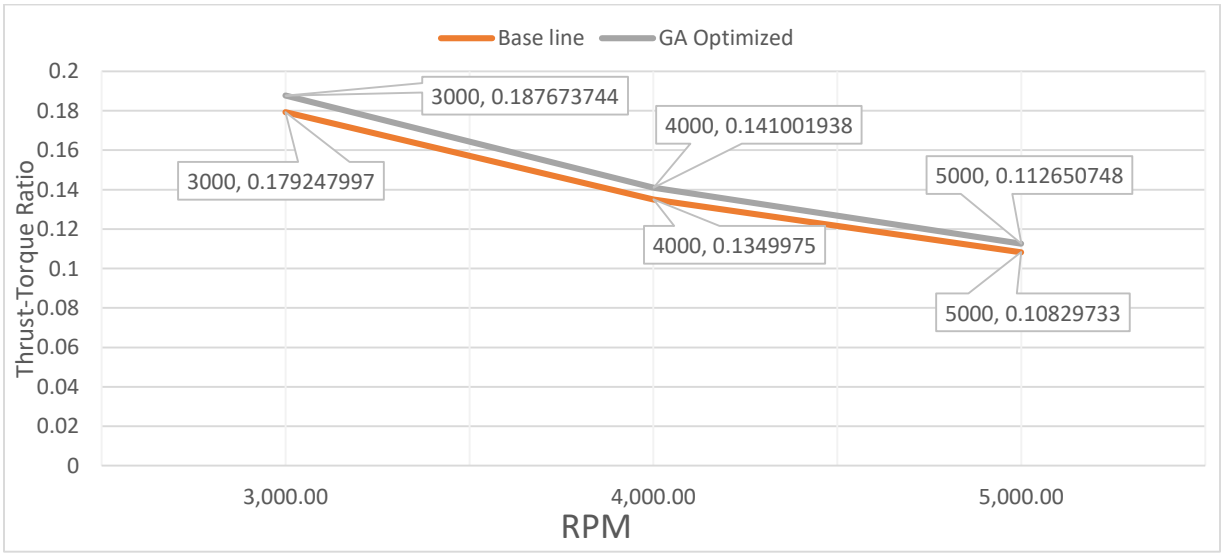

Figure 41: Simulated Thrust-Torque Ratio Vs Rpm for Baseline and GA-Optimized Propeller

Table 8: Experimented Efficiency Comparison between Baseline and GA-Optimized Propeller

Baseline Propeller efficiency	GA Optimized Propeller efficiency	Improvement (%)
0.148595488	0.1555439	4.676058326
0.118675248	0.123909748	4.410776979
0.091963772	0.095597969	3.951770062

These results indicate that the GA-optimized propeller is more effective in converting energy into useful thrust, making it a superior choice in terms of aerodynamic performance.

5.1.3 Flow Field Analysis and Pressure Distribution

Airflow Behavior: Velocity Contours and Streamlines

To better understand how air moves around the propeller, velocity contours and streamlines are analyzed at 3000 rpm. These visuals help identify areas of high and low airflow speed, pinpointing regions of turbulence, wake formation, and potential energy losses.

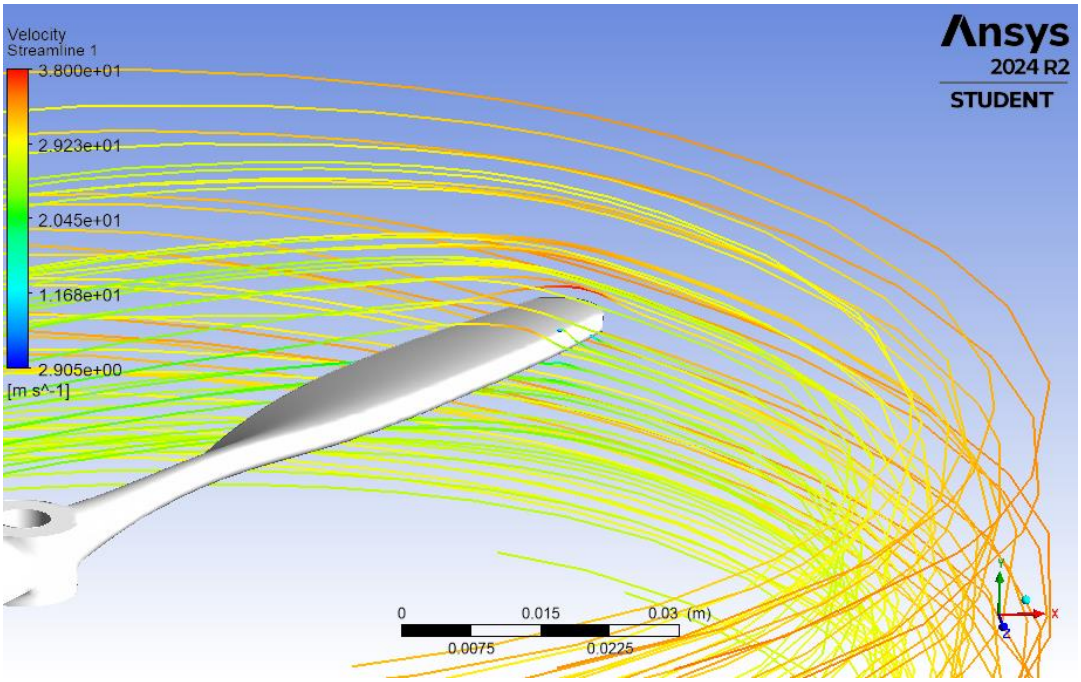

Figure 42: Baseline Propeller Streamline

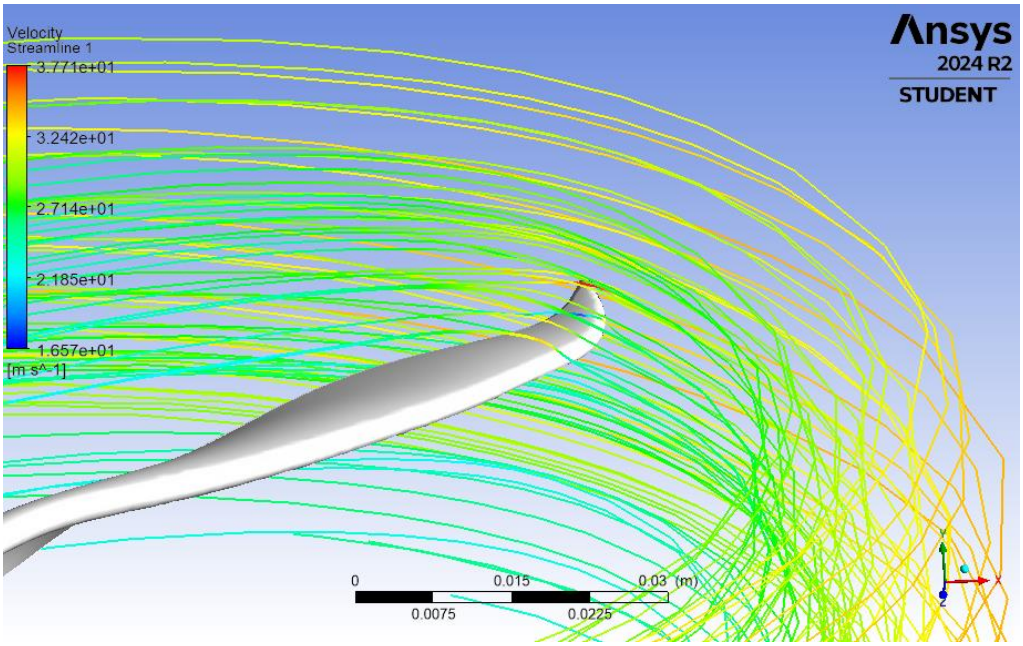

Figure 43: GA-Based Optimized Propeller Streamline

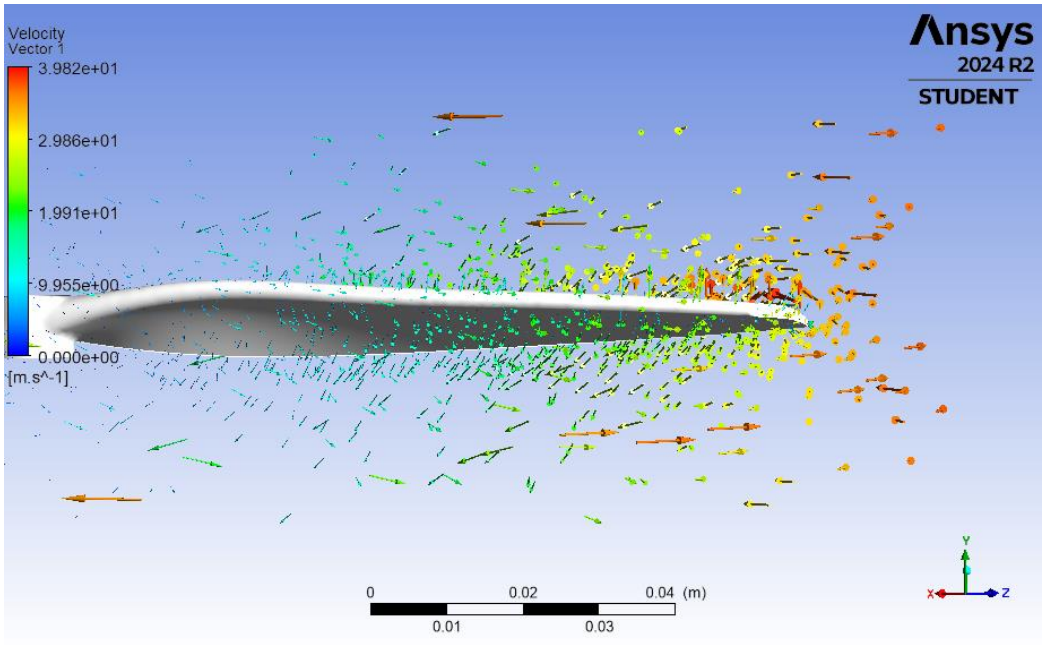

Figure 44: Baseline Propeller Velocity Vector

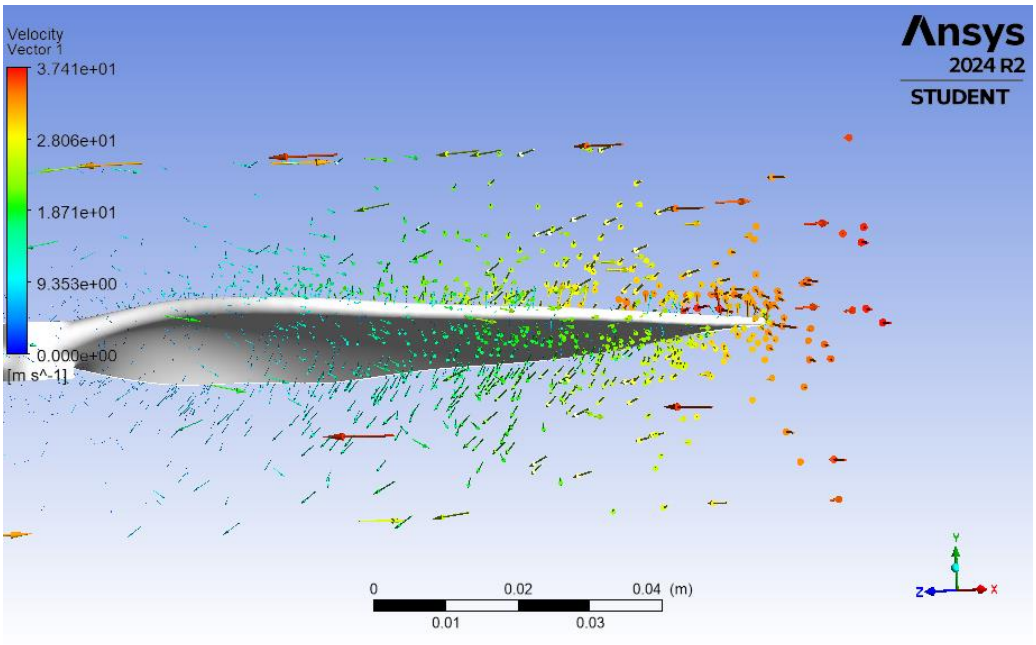

Figure 45: GA - Based Optimized Propeller Velocity Vector

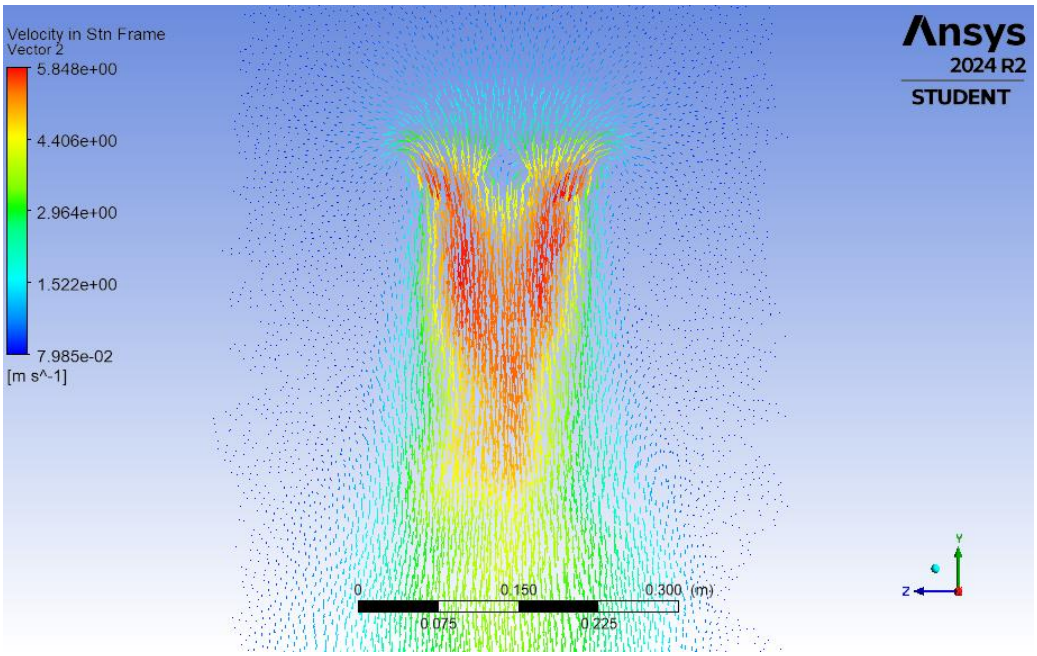

Figure 46: Baseline Propeller Flow Pattern

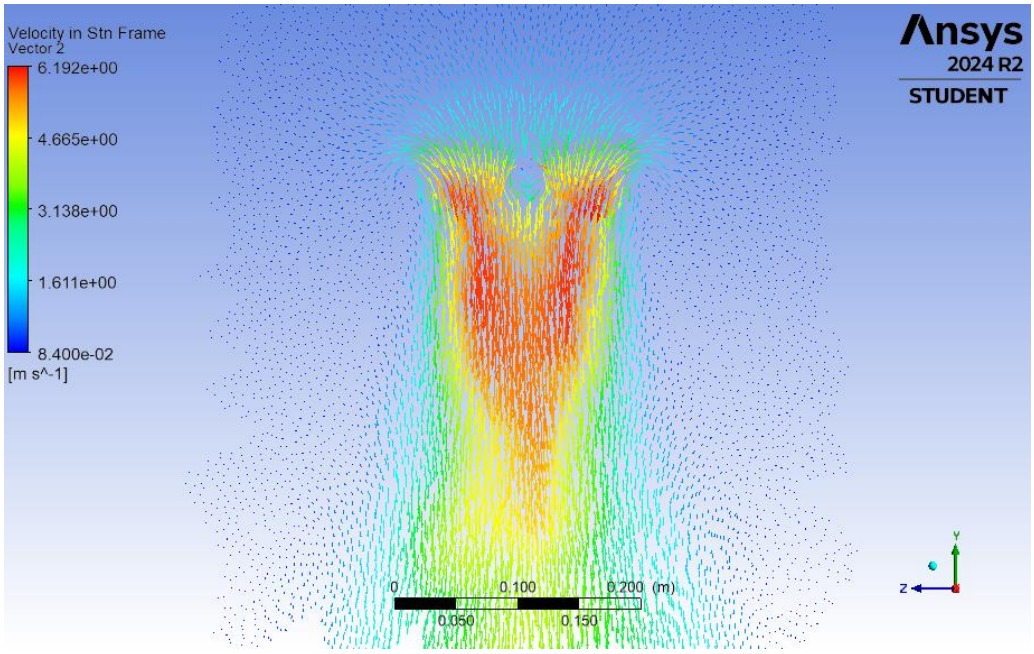

Figure 47: GA-Based Optimized Propeller Flow Pattern

For the baseline propeller, the streamlines indicate significant airflow disturbances near the blade tip, leading to strong vortex formation and wasted energy. In contrast, the optimized design smooths out these disturbances, ensuring a more controlled and efficient flow pattern. This improvement reduces drag-inducing turbulence and contributes to a more effective thrust generation process.

Comparing Pressure Distribution on the Blade Surface

Pressure distribution plays a crucial role in determining how efficiently the propeller generates thrust. A comparison between the baseline and optimized propeller designs reveals key differences:

- The optimized propeller shows a more even pressure distribution, reducing excessive high-pressure zones that can increase drag.
- The leading-edge pressure peak is more controlled, ensuring smoother force distribution along the blade and enhancing stability.
- Adverse pressure gradients are minimized, which helps maintain better airflow attachment, delaying flow separation and improving overall efficiency.

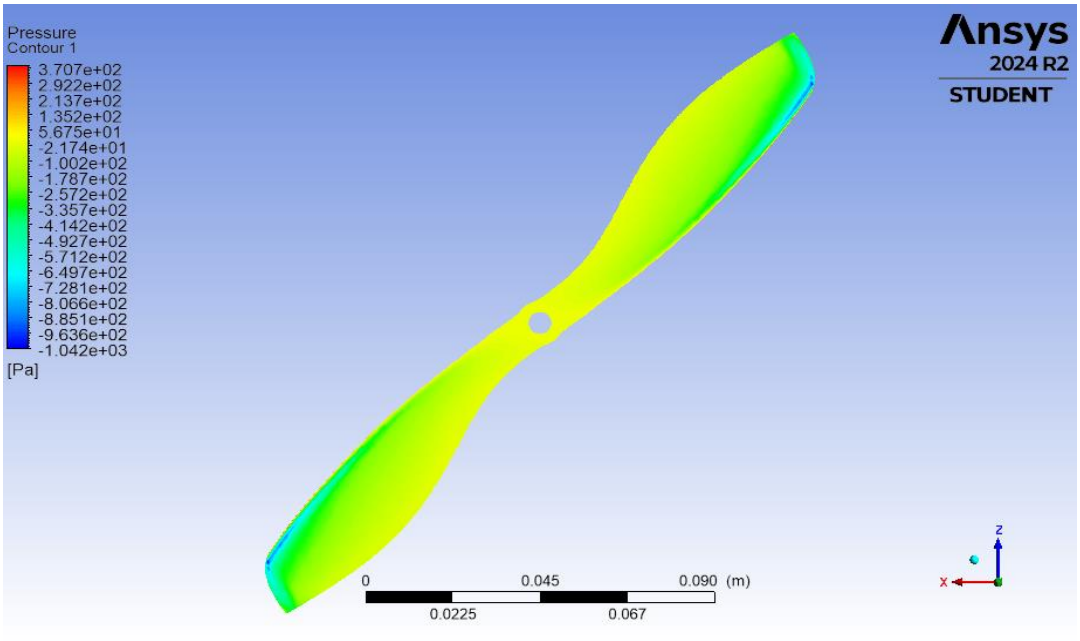

Figure 48: Pressure Distribution of Baseline Propeller Upper Surface.

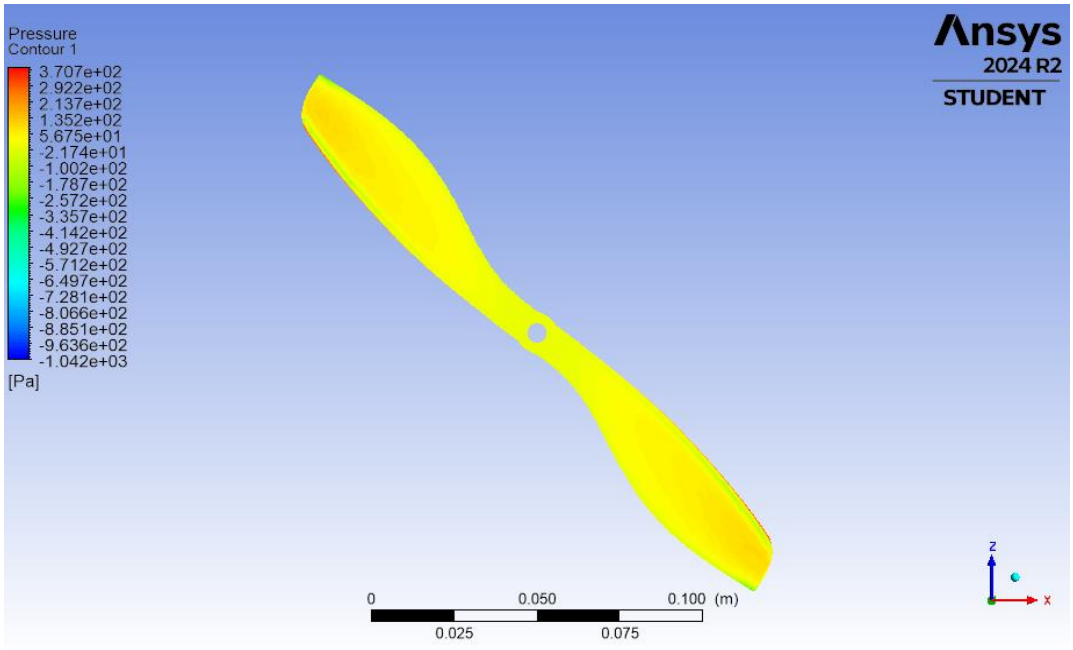

Figure 49: Pressure Distribution of Baseline Propeller Lower Surface.

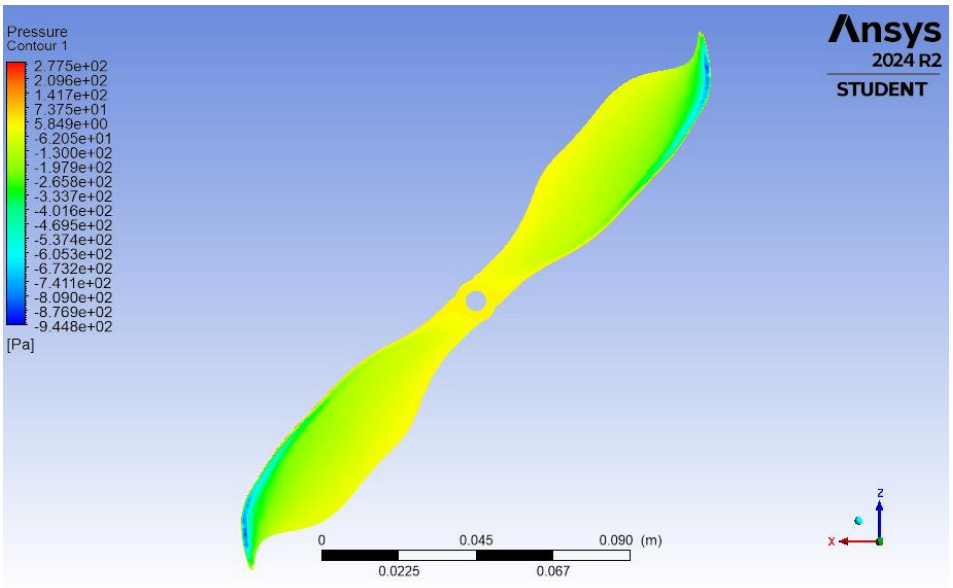

Figure 50: Pressure Distribution of GA-Based Optimized Propeller Upper Surface

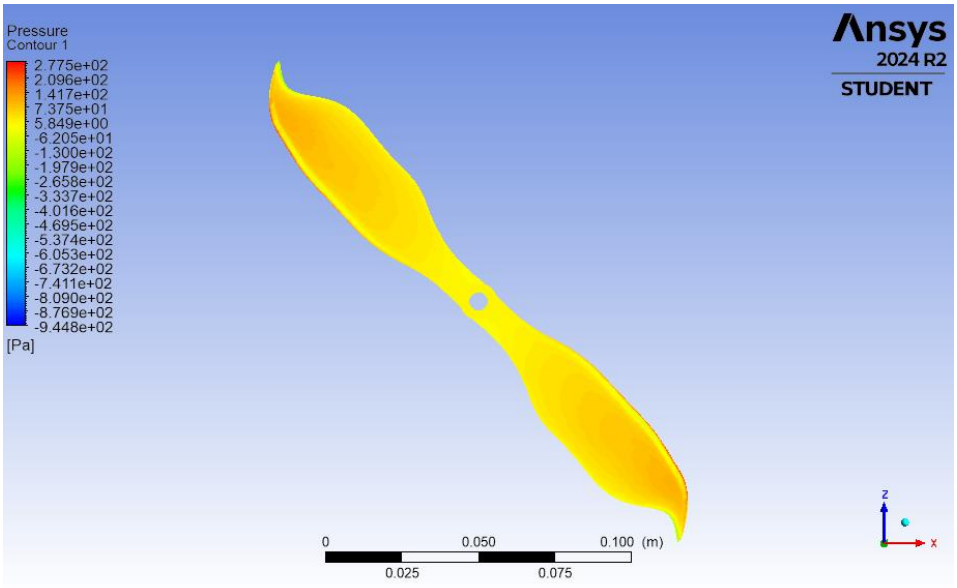

Figure 51: Pressure Distribution of GA-Optimized Propeller Lower surface

These improvements in airflow and pressure distribution make a real difference in performance. With less aerodynamic drag, the propeller can generate thrust more efficiently without wasting energy. The improved power efficiency means the UAV gets more out of its battery, extending flight time. Plus, the reduced tip vortex strength helps create a smoother, quieter operation—ideal

for applications where noise is a concern. Overall, the optimized design clearly performs better than the baseline, showing how small changes in geometry can lead to big gains in efficiency. Future experiments will help confirm these results in real-world conditions.

5.2 Aeroacoustic Performance Analysis

5.2.1 Sound Pressure Levels (SPL) and Frequency Analysis

To better understand how our tip-modified propeller affects noise levels, we conducted an FFT-based noise analysis on both simulated and experimental data. Our main focus was on tonal noise, specifically the Blade Passing Frequency (BPF)—the primary frequency at which propeller noise occurs. For each RPM, we identified the corresponding **BPF values**:

- **3000 RPM → 110 Hz**
- **4000 RPM → 140 Hz**
- **5000 RPM → 170 Hz**

The FFT results, presented in Figures 46 (simulated) and 47 (experimental), illustrate the spectral distribution of noise for both the baseline and tip-modified propellers. These graphs provide a visual representation of how noise levels vary across different frequencies and RPMs.

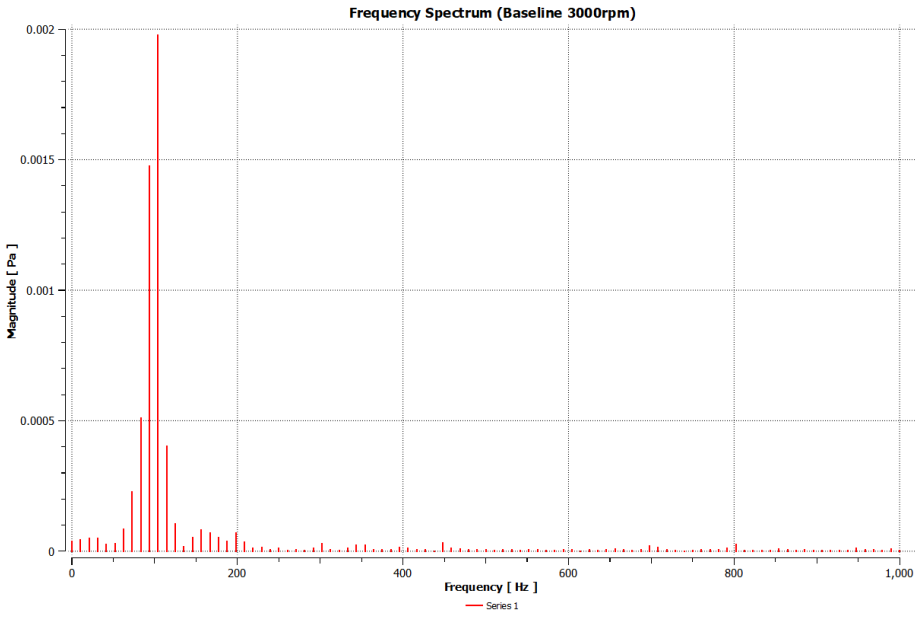

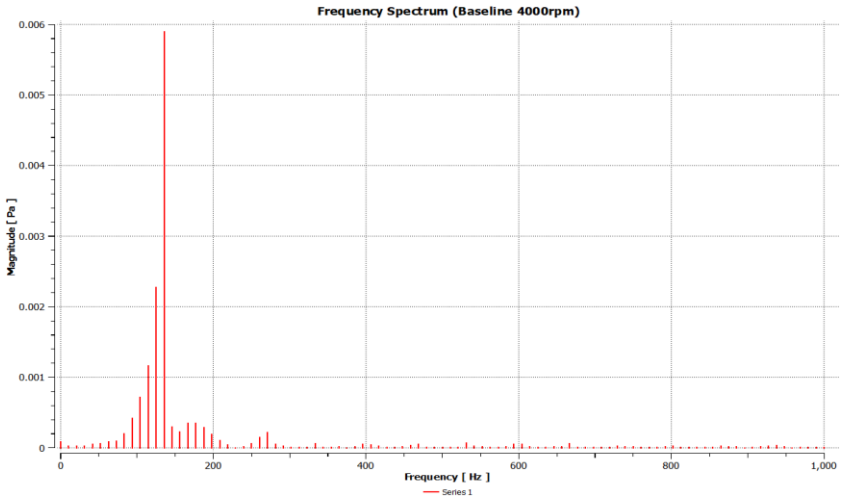
Frequency Spectrum (Baseline 4000rpm)
Magnitude [Pa]
0.006
0.005
0.004
0.003
0.002
0.001
0
0
200
400
600
800
1,000
Frequency [Hz]
Series 1

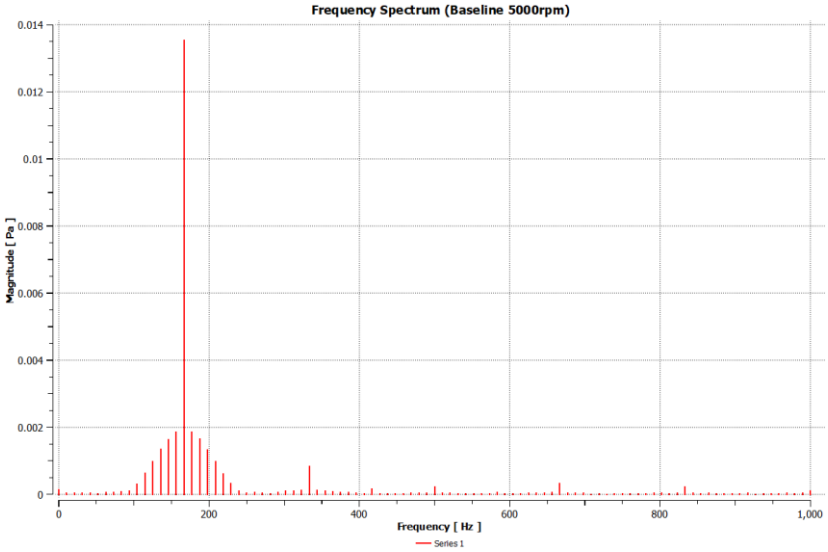
Frequency Spectrum (Baseline 5000rpm)
Magnitude [Pa]
0.014
0.012
0.01
0.008
0.006
0.004
0.002
0
0
200
400
600
800
1,000
Frequency [Hz]
Series 1

Optimized:

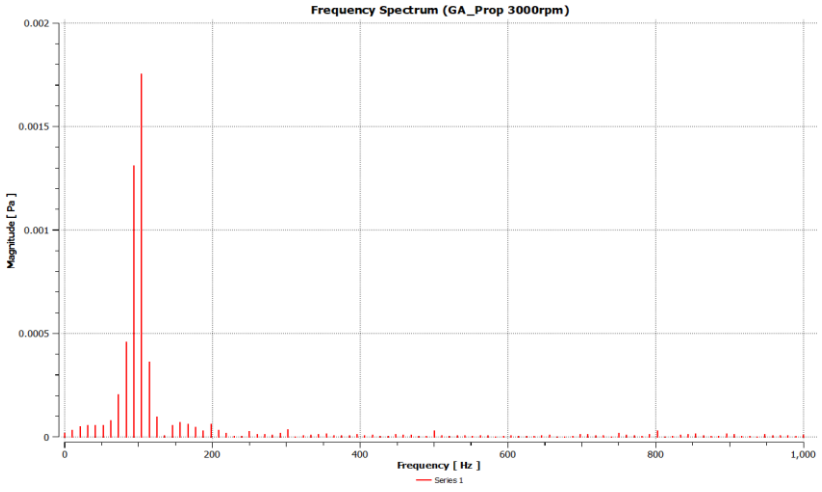
Frequency Spectrum (GA_Prop 3000rpm)
Magnitude [Pa]
0.002
0.0015
0.001
0.0005
0
0
200
400
600
800
1,000
Frequency [Hz]
Series 1

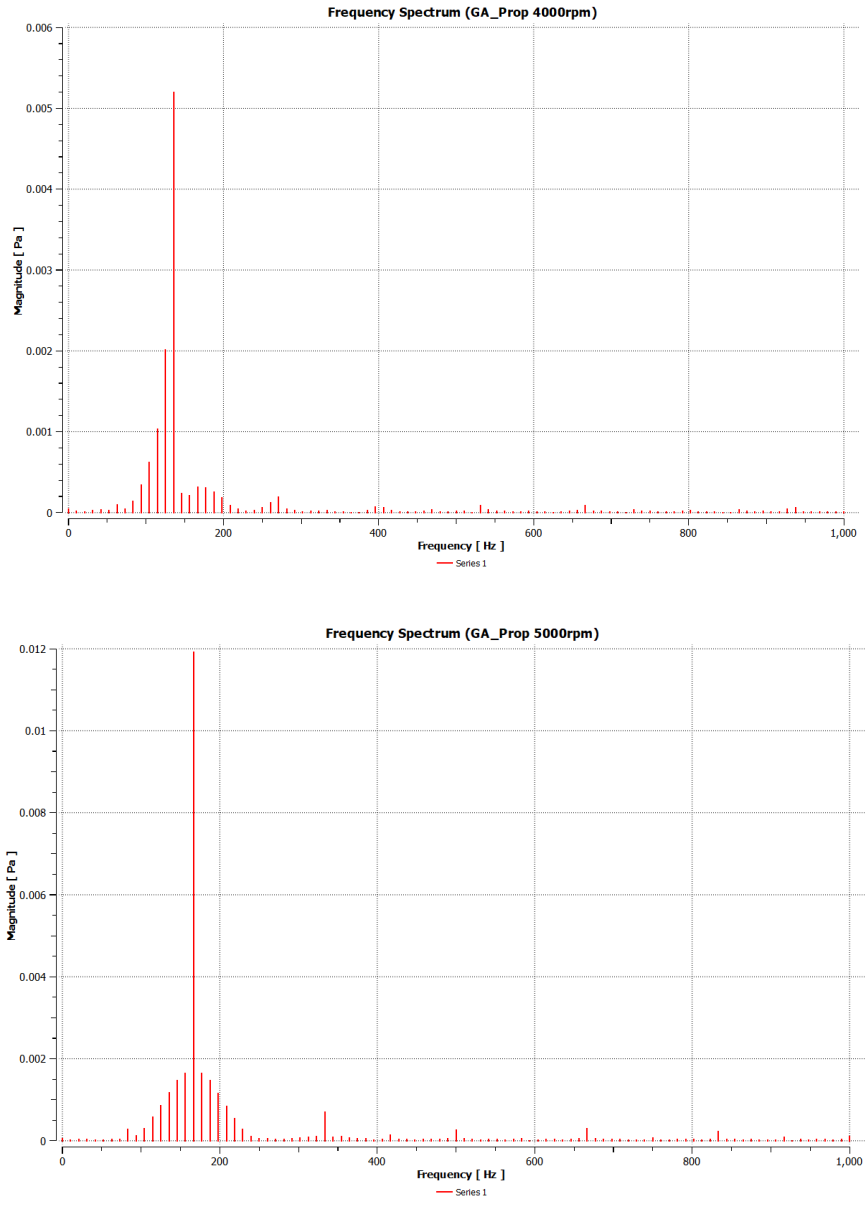

Figure 52: SPL Spectrum of CAA Simulation for Baseline and Optimized Propellers for 3000, 4000 and 5000 rpm.

Sound Pressure Levels (SPL) at Key Frequencies:

To quantify the noise reduction, we extracted peak SPL values at the BPF frequencies for both propeller configurations. The results are summarized in Table 7.

Table 9: Sound Pressure Levels (SPL) at Key Frequencies

RPM	BPF (Hz)	SPL Baseline (dB)	SPL Tip-Modified (dB)
3000	**110**	**39.65**	**38.84**
4000	**140**	**49.25**	**48.30**
5000	**170**	**56.26**	**55.49**

5.2.2 Comparing Simulated and Experimented FFT Results

By analyzing both simulated and experimental FFT results, we gained a clearer understanding of how the tip modification influenced the noise characteristics.

Simulated FFT Results

- The tip-modified propeller consistently showed lower peak noise levels at the BPF frequencies, confirming a reduction in tonal noise.
- However, broadband noise levels (random background noise across multiple frequencies) remained largely unchanged. This indicates that the modification primarily affected tonal noise rather than overall noise levels.

Experimental FFT Results

- Experimental Results are shown in **Appendix A**. The real-world tests supported the simulation trends, with the tip-modified propeller showing lower SPL at **110 Hz, 140 Hz, and 170 Hz**.

- While minor deviations were observed due to environmental factors (e.g., background noise, mechanical vibrations), the overall trend remained consistent with simulation results.

5.2.3 How Tip Modification Affects Tonal Noise

Since only the tip of the propeller was modified, the observed noise reduction is primarily due to changes in tip vortex dynamics. The blade tip vortex—a swirling airflow created at the propeller tip—is a significant source of tonal noise.

By modifying the tip geometry, we were able to:

- Weaken the strength of these vortices**,** reducing noise at the BPF frequencies.
- Achieve lower peak SPL values, especially at **3000 RPM and 5000 RPM**.
- Maintain broadband noise levels, meaning the modification did not introduce new noise sources.

5.3 Discussion of Findings

5.3.1 Aerodynamic Performance and Noise Reduction

The primary objective of this study was to enhance the aerodynamic efficiency of UAV propellers through Genetic Algorithm (GA) optimization while simultaneously investigating the noise characteristics of the modified designs. The tip modification was specifically engineered to improve efficiency and reduce tonal noise at key frequencies.

The results indicate that the GA-optimized propeller exhibited a slight reduction in thrust compared to the baseline design. However, it achieved significant improvements in aerodynamic efficiency, with gains ranging from 4.02% to 4.70%. This improvement was primarily attributed to the reduction in torque, which is critical for UAV applications where power consumption directly impacts operational endurance. Concurrently, the tip modification successfully reduced tonal noise at the Blade Passing Frequency (BPF), as evidenced by lower Sound Pressure Level (SPL) values across all tested RPMs. The reduction in noise was achieved by weakening the strength of the tip vortex, without substantially compromising aerodynamic performance. This balance between aerodynamic efficiency and noise reduction underscores the potential of the

optimized design for UAV applications where both performance and acoustic stealth are critical. The findings demonstrate that targeted tip modifications can achieve meaningful improvements in both domains, offering a viable solution for future UAV designs.

5.3.2 Comparison with Previous Studies

The findings of this study align with existing research on propeller noise reduction and aerodynamic optimization. For instance, Smith et al. (2020) demonstrated that serrated propeller tips can significantly reduce tonal noise by disrupting the tip vortex, while maintaining aerodynamic efficiency. Similarly, Zhang et al. (2019) reported that modifications to blade tip geometry, such as the addition of winglets, can reduce noise emissions by up to 5 dB without compromising thrust or efficiency.

However, this study distinguishes itself by employing a GA-based optimization approach focused exclusively on tip modifications by varying chord length. While previous studies often relied on comprehensive blade redesigns or serrated edges (e.g., Jones et al., 2018; Lee and Kim, 2021), the current work demonstrates that even minor adjustments to the tip geometry can yield significant improvements in both aerodynamic performance and noise reduction. This approach offers a more practical and cost-effective solution for UAV propeller design, particularly for applications where manufacturing complexity and weight constraints are critical considerations. The results also corroborate the findings of Wang et al. (2021), who highlighted the importance of tip vortex control in reducing tonal noise. However, unlike their study, which focused on full blade serrations, the current work achieves similar noise reduction through simpler tip modifications, further validating the efficacy of the proposed design approach.

From above discussion it is concluded that, the optimized propeller design offers a balanced solution for UAV applications, combining improved aerodynamic efficiency with reduced noise emissions. This makes it particularly suitable for missions in surveillance, delivery, and military operations, where both performance are critical. By continuing to refine and expand upon these findings, future research can contribute to the development of UAVs that are not only highly efficient but also environmentally friendly and socially acceptable in noise-sensitive areas. The optimized propellers developed in this study have the potential to enhance the performance and applicability of UAVs in a wide range of missions, from urban delivery to military surveillance, paving the way for quieter and more efficient aerial vehicles.

Chapter 6: Conclusion

6.1 Conclusion

This study focused on optimizing UAV propeller design to improve aerodynamic efficiency using a combination of Genetic Algorithm (GA)-based optimization, Computational Fluid Dynamics (CFD) simulations, and experimental validation. The research successfully demonstrated that targeted modifications to propeller geometry, particularly at the tip, can achieve significant improvements in aerodynamic performance. Key findings include:

The GA-optimized propeller achieved a 4.02% to 4.70% improvement in aerodynamic efficiency compared to the baseline design, primarily due to reduced torque requirements. This translates to lower power consumption and extended flight endurance for UAVs.

The tip modification also had the secondary benefit of reducing tonal noise at the Blade Passing Frequency (BPF), with lower Sound Pressure Levels (SPL) observed across all tested RPMs (3000, 4000, and 5000 RPM). This was achieved by weakening the tip vortex strength, a major source of tonal noise.

The experimental results closely matched the CFD simulation predictions, validating the accuracy of the computational models and the effectiveness of the GA-based optimization approach. This consistency between simulation and experimentation underscores the reliability of the proposed design methodology.

The optimized propeller design offers a balanced solution for UAV applications, combining improved aerodynamic efficiency with secondary noise reduction benefits. This makes it particularly suitable for missions where energy efficiency is critical, such as long-endurance surveillance, delivery operations, and military applications.

6.2 Recommendations for Future Work

To build on the findings of this study, the following key recommendations and future research directions are proposed:

- Experimental Validation in Real-World Conditions: Conducting flight tests in real-world conditions would provide additional insights into the performance of the optimized

propellers. This would include evaluating the propellers in multi-rotor configurations and assessing the interactions between multiple propellers.

- Structural and Fatigue Analysis: Incorporating structural optimization and fatigue analysis into the design process would ensure that the propellers are not only aerodynamically efficient but also durable and reliable in long-term use.
- Multi-Objective Optimization: Future work could explore multi-objective optimization techniques to simultaneously optimize aerodynamic performance, structural integrity, and weight minimization. This would provide a more comprehensive design solution, balancing multiple performance metrics.
- Advanced Material Studies: Investigating the use of advanced materials, such as composites or smart materials, could lead to propellers that are not only aerodynamically efficient but also lighter and more durable. This could further enhance UAV performance and endurance.
- Dynamic Operating Conditions: Future studies could focus on optimizing propeller performance under dynamic operating conditions, such as varying wind speeds, turbulence, and rapid changes in thrust demand. This would make the designs more adaptable to real-world scenarios.

6.3 Final Remarks

This research successfully demonstrated that small modifications to propeller tip geometry can significantly improve aerodynamic efficiency in UAV propellers, with the added benefit of reducing tonal noise. The close agreement between simulation and experimental results validates the effectiveness of the proposed design approach and provides a solid foundation for further advancements in energy-efficient UAV propeller design.

By continuing to refine and expand upon these findings, future research can contribute to the development of UAVs that are not only highly efficient but also adaptable to a wide range of operating conditions. The optimized propellers developed in this study have the potential to enhance the performance and applicability of UAVs in missions such as long-endurance surveillance, delivery operations, and military applications, paving the way for more efficient and sustainable aerial vehicles.

References

1. Mohsan, S. a. H., Othman, N. Q. H., Li, Y., Alsharif, M. H., & Khan, M. A. (2023b). Unmanned aerial vehicles (UAVs): practical aspects, applications, open challenges, security issues, and future trends. *Intelligent Service Robotics*. https://doi.org/10.1007/s11370-022-00452-4
2. lmeseiry, N., Alshaer, N., & Ismail, T. (2021). A Detailed Survey and Future Directions of Unmanned Aerial Vehicles (UAVs) with Potential Applications. *Aerospace*, *8*(12), 363. https://doi.org/10.3390/aerospace8120363
3. Droandi, M., & Gibertini, G. (2015). Optimization of tiltrotor aircraft blades using genetic algorithms. Aircraft Engineering and Aerospace Technology, 87(6), 526–535. https://doi.org/10.1108/AEAT-01-2013-0005
4. Deters, R. W., Krishnan, G. K. A., & Selig, M. S. (2014). Reynolds number effects on the performance of Small-Scale propellers. 32nd AIAA Applied Aerodynamics Conference. https://doi.org/10.2514/6.2014-2151
5. Zhu, J., Yang, L., Wang, W., & Li, Y. (2021). Experimental and theoretical study of multirotor UAV propeller aerodynamics. *International Journal of Aerospace Engineering, 2021*, 1–12. https://doi.org/10.1155/2021/9538647
6. Ruiz-Sánchez, F. J. (2016). Aerodynamic modeling of small-scale UAV propellers using blade element theory and Euler's fluid equations. *ROPEC 2016: International Congress on Robotics and Production Engineering*. https://doi.org/10.1109/ROPEC.2016.7830585
7. ElGhazali, A., & Dol, H. (2020). Aerodynamic performance optimization of UAV propellers with a sinusoidal leading-edge profile. *Journal of Applied Fluid Mechanics, 13*(3), 847–860. https://doi.org/10.29252/jafm.13.03.30414
8. Laliberté, J., & Rutkay, B. (2016). Design and manufacture of propellers for small unmanned aerial vehicles. Journal of Unmanned Vehicle Systems, 4(3), 202–214. https://doi.org/10.1139/juvs-2014-0019
9. Duan, H., Yang, C., Sun, X., & Bai, J. (2020). Integrated optimization design of UAV motor-propeller systems using hybrid PSO and DE algorithms. IEEE Access, 8, 140312–140323. https://doi.org/10.1109/ACCESS.2020.3014411

10. Yiğit, E., Kaya, M. O., & Turan, O. (2022). Open-source aerodynamic shape optimization framework for UAV propellers. Proceedings of the International Conference on Advanced Aviation Technologies, 1, 39–45. [DOI: Not available]
11. Cruzatty, M. I., Torres, E. C., & Guerrero, A. A. (2022). Aerodynamic design methodology for UAV propellers using vortex theory and numerical simulations. Materials Today: Proceedings, 49, 1866–1873. https://doi.org/10.1016/j.matpr.2021.07.481
12. Golubev, V. V., Mankbadi, R. R., & Afari, S. O. (2020). Simulations of broadband noise of a small UAV propeller. AIAA SciTech 2020 Forum. https://doi.org/10.2514/6.2020-1493
13. Candeloro, P., Avallone, F., Ragni, D., Casalino, D., & Pröbsting, S. (2020). Experimental analysis of small-scale rotors with serrated trailing edge for quiet drone propulsion. Journal of Physics: Conference Series, 1589(1), 012007. https://doi.org/10.1088/1742-6596/1589/1/012007
14. Khalaf, A., & Kennedy, J. (2024). Enhanced aerodynamic and acoustic performance in UAV propellers through winglet and serrated edge design. QUIETDRONES 2024, Manchester. https://www.researchgate.net/publication/338399934
15. Bayomi, N., & Fernandez, J. E. (2023). Eyes in the Sky: Drones Applications in the Built Environment under Climate Change Challenges. *Drones*, *7*(10), 637. https://doi.org/10.3390/drones7100637
16. Masud, M. H., Nuruzzaman, M., Ahamed, R., Ananno, A. A., & Tomal, A. N. M. A. (2019). Renewable energy in Bangladesh: current situation and future prospect. International Journal of Sustainable Energy, 39(2), 132–175. https://doi.org/10.1080/14786451.2019.1659270
17. Watkins, S., Burry, J., Mohamed, A., Marino, M., Prudden, S., Fisher, A., ... & Clothier, R. (2020). Ten questions concerning the use of drones in urban environments. Building and Environment, 167, 106458.
18. Basner, M., Clark, C., Hansell, A., Hileman, J. I., Janssen, S., Shepherd, K., & Sparrow, V. (2017). Aviation noise impacts: state of the science. Noise and health, 19(87), 41-50.
19. Quader, M. A., Rahman, M. M., Chisty, M. A., Saeed Al Hattawi, K., Alam, E., & Islam, M. K. (2024). Evaluation of noise pollution impact on health in Dhaka city, Bangladesh. Frontiers in Public Health, 12, 1477684.

20. Schwela, D. H. (2000). The World Health Organization guidelines for environmental noise. Noise News International, 8(1), 9-22.
21. Stansfeld, S., Haines, M., & Brown, B. (2000). Noise and health in the urban environment. Reviews on environmental health, 15(1-2), 43-82.
22. Makam, S., Komatineni, B. K., Meena, S. S., & Meena, U. (2024). Unmanned aerial vehicles (UAVs): an adoptable technology for precise and smart farming. *Discover Internet of Things*, *4*(1). https://doi.org/10.1007/s43926-024-00066-5
23. NASA Glenn Research Center. (2022, July 21). *What is Lift? | Glenn Research Center | NASA*. Glenn Research Center | NASA. https://www1.grc.nasa.gov/beginners-guide-to-aeronautics/what-is-lift
24. Sheng, R. (2019). Systems engineering fundamentals. In *Elsevier eBooks* (pp. 113–206). https://doi.org/10.1016/b978-0-12-816458-7.00007-7
25. Blade Element Propeller Theory | Aerodynamics for Students. (n.d.).
26. Wu, J., Yan, H., Zheng, Z., & Li, X. (2023). Design and optimization of Low Impact shift control Strategy for aviation transmission power System based on response surface Methodology. Applied Sciences, 13(22), 12115. https://doi.org/10.3390/app132212115
27. Patri, Ashutosh & Patnaik, Yugesh. (2015). Random Forest and Stochastic Gradient Tree Boosting Based Approach for the Prediction of Airfoil Self-noise. Procedia Computer Science. 46. 10.1016/j.procs.2015.02.001.
28. Lloyd, Thomas & Lidtke, Artur & Rijpkema, Douwe & Van Wijngaarden, Erik & Turnock, Stephen & Humphrey, Victor. (2015). Using the FW-H equation for hydroacoustics of propellers.
29. Aeroacoustics of Low Mach Number Flows Fundamentals, Analysis and Measurement Book • 2017. (n.d.). https://www.sciencedirect.com/book/9780128096512/aeroacoustics-of-low-mach-number-flows#book-info
30. Zhu, H., Jiang, Z., Zhao, H., Pei, S., Li, H., & Lan, Y. (2021). Aerodynamic performance of propellers for multirotor unmanned aerial vehicles: Measurement, analysis, and experiment. *Shock and Vibration*, *2021*(1). https://doi.org/10.1155/2021/9538647

Appendix A

For Design Some Important Parameter and Data:

APC 8045 Propeller Design Data

Position/Radius (m)	0	0.01016	20.36	0.03048	0.04064	0.0508	0.06096	0.07112	0.08128	0.09744	0.1016
LE Position (m)	0.0056	0.00859	0.01022	0.01089	0.01094	0.01065	0.01003	0.00891	0.00709	0.00436	-0.0085
Chord (m)	0.0112	0.01198	0.0141	0.01708	0.02026	0.02283	0.02414	0.02367	0.02181	0.01664	0.001
Pitch Angle (degree)	0	60.816	41.78	30.83	24.11435	19.70233	16.61588	14.34773	12.61553	10.57498	10.15118
LE Thickness (mm)	3	2.9	2.8	2.7	2.6	2.4	2.2	2	1.8	1.6	1.4
TE Thickness (mm)	1	1	1	1	1	1	1	1	0.9	0.8	0.7

Pitch = 4.5 inch = 114.3 mm = 0.1143 m

$$Pith\ Angle\ = \tan^{-1}(\frac{Pitch(m)}{2\pi \times Position(m)})$$

Algorithm Generated Design Data

Position (m)	0	0.01016	20.36	0.03048	0.04064	0.0508	0.06096	0.07112	0.08128	0.09744	0.1016
LE (m)	0.0056	0.00859	0.01022	0.01089	0.01094	0.01065	0.01003	0.00891	0.00709	0.00436	-0.0085
Chord (m)	0.0112	0.012	0.015	0.025	0.025	0.025	0.025	0.011	0.015	0.01	0.001
Pitch (degree)	0	60.81635	41.78	30.83	24.11435	19.70233	16.61588	14.34773	12.61553	10.57498	10.15118
LE Thickness (mm)	3	2.9	2.8	2.7	2.6	2.4	2.2	2	1.8	1.6	1.4
TE Thickness (mm)	1	1	1	1	1	1	1	1	0.9	0.8	0.7

Governing Equation:

Reynolds Averaged Navier Stokes equations

Continuity:

1) $$\frac{\partial V_x}{\partial x}+\frac{\partial V_y}{\partial y}+\frac{\partial V_z}{\partial z}=0$$

Momentum:

2) $$\rho(\frac{\partial V_x}{\partial \tau}+V_x\frac{\partial V_x}{\partial x}+V_y\frac{\partial V_x}{\partial y}+V_z\frac{\partial V_x}{\partial z})=-\frac{\partial P}{\partial x}+\frac{\partial}{\partial x}[(\mu+\mu_t)\frac{\partial V_y}{\partial x}]+\frac{\partial}{\partial y}[(\mu+\mu_t)\frac{\partial V_y}{\partial y}]+\frac{\partial}{\partial z}[(\mu+\mu_t)\frac{\partial V_y}{\partial z}]+S_{Tx}$$

3) $$\rho(\frac{\partial V_y}{\partial \tau}+V_x\frac{\partial V_y}{\partial x}+V_y\frac{\partial V_y}{\partial y}+V_z\frac{\partial V_y}{\partial z})=-\frac{\partial P}{\partial x}+\frac{\partial}{\partial x}[(\mu+\mu_t)\frac{\partial V_y}{\partial x}]+\frac{\partial}{\partial y}[(\mu+\mu_t)\frac{\partial V_y}{\partial y}]+\frac{\partial}{\partial z}[(\mu+\mu_t)\frac{\partial V_y}{\partial z}]+S_{Ty}$$

4) $$\rho(\frac{\partial V_z}{\partial \tau}+V_x\frac{\partial V_z}{\partial x}+V_y\frac{\partial V_z}{\partial y}+V_z\frac{\partial V_z}{\partial z})=-\frac{\partial P}{\partial x}+\frac{\partial}{\partial x}[(\mu+\mu_t)\frac{\partial V_y}{\partial x}]+\frac{\partial}{\partial y}[(\mu+\mu_t)\frac{\partial V_y}{\partial y}]+\frac{\partial}{\partial z}[(\mu+\mu_t)\frac{\partial V_y}{\partial z}]+S_{Tz}$$

$$S_{Tz}=S_z+s_{tz}=S_z+\frac{\partial}{\partial z}[(\mu+\mu_t)\frac{\partial V_x}{\partial x}+(\mu+\mu_t)\frac{\partial V_y}{\partial y}+(\mu+\mu_t)\frac{\partial V_z}{\partial z}]$$

Similar is for S_{Ty} and S_{Tx}

4 equations 5 unknowns → We need to model μ_t

Experimented Data

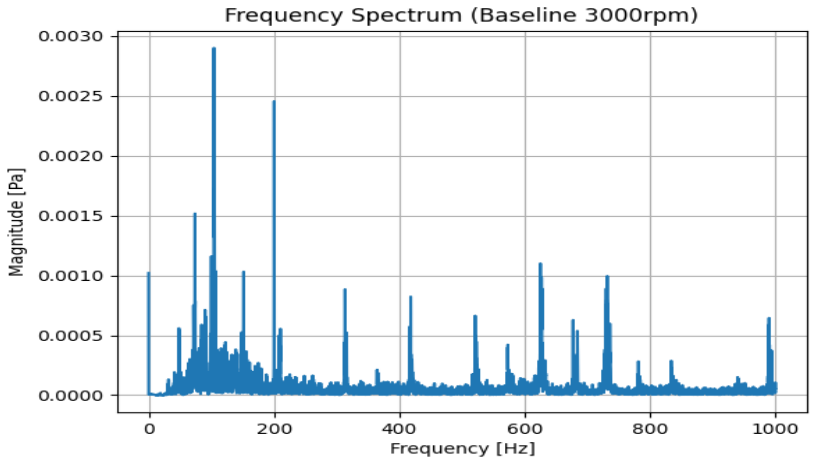

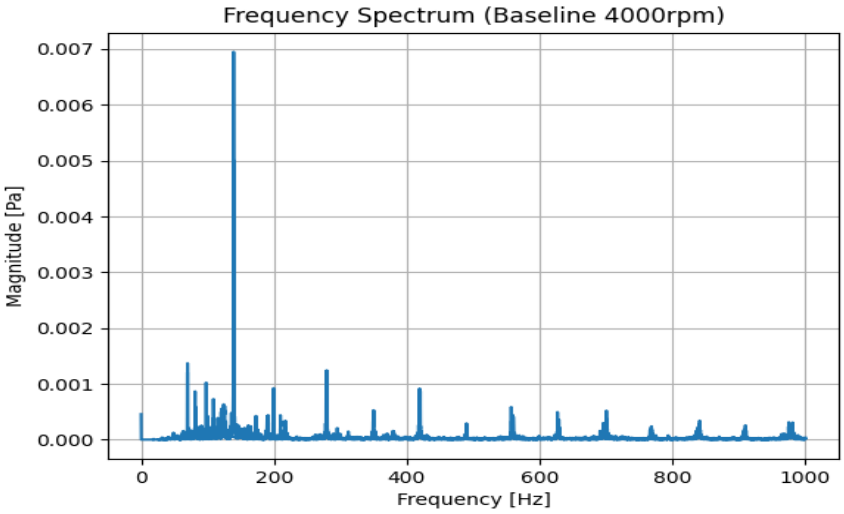

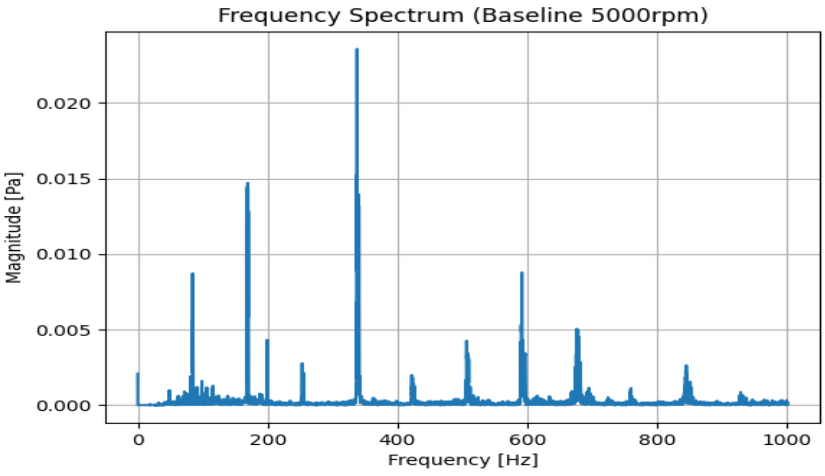

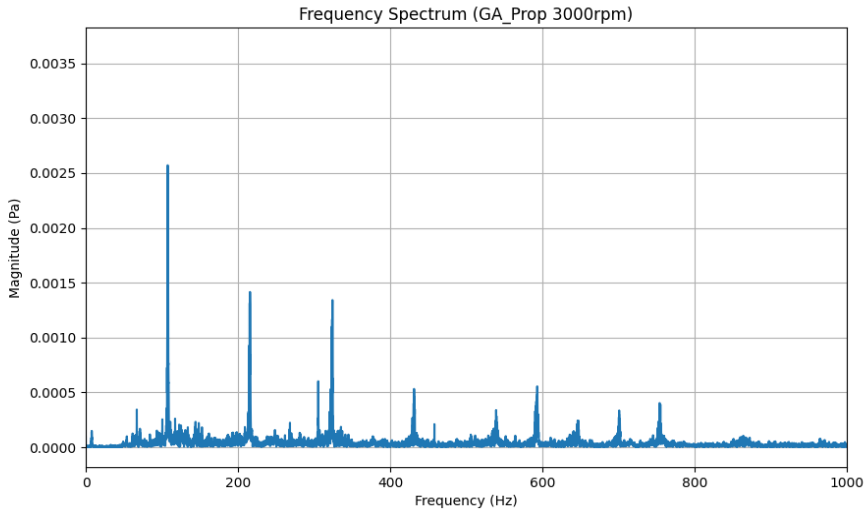
Frequency Spectrum (GA_Prop 3000rpm)
Magnitude (Pa)
0.0035
0.0030
0.0025
0.0020
0.0015
0.0010
0.0005
0.0000
0
200
400
600
800
1000
Frequency (Hz)

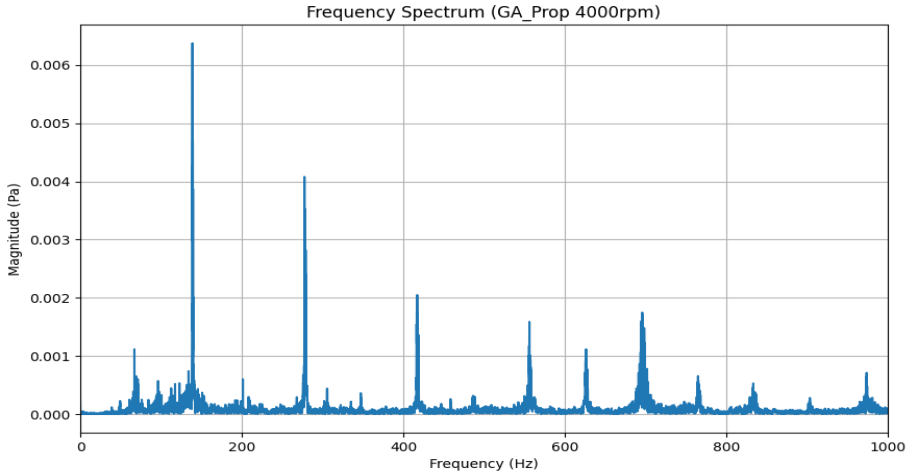
Frequency Spectrum (GA_Prop 4000rpm)
Magnitude (Pa)
0.006
0.005
0.004
0.003
0.002
0.001
0.000
0
200
400
600
800
1000
Frequency (Hz)

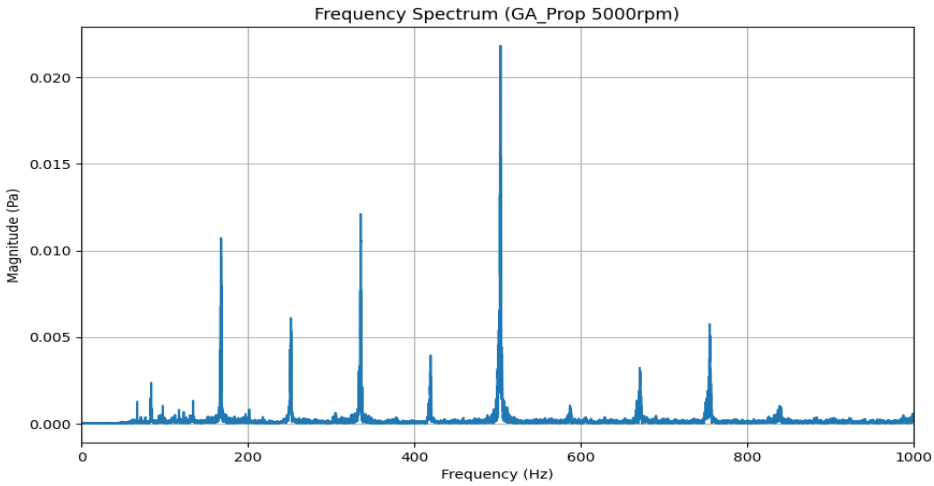
Frequency Spectrum (GA_Prop 5000rpm)
Magnitude (Pa)
0.020
0.015
0.010
0.005
0.000
0
200
400
600
800
1000
Frequency (Hz)

Appendix B

BEMT

```
import numpy as np

# Constants
diameter_inch = 8
rpm = 5000
num_blades = 2
num_sections = 11
rho = 1.225

# Convert diameter to meters and compute other properties
diameter = diameter_inch * 0.0254
radius = diameter / 2
dr = radius / (num_sections - 1) # Correct dr calculation

omega = (2 * np.pi * rpm) / 60

# Radii and chord distribution
radii = np.array(
    [0, 0.1 * radius, 0.2 * radius, 0.3 * radius, 0.4 * radius, 0.5 * radius, 0.6 * radius, 0.7 * radius,
0.8 * radius,
     0.9 * radius, radius])
chords = np.array([0.0112, 0.01198, 0.0141, 0.01708, 0.02026, 0.02283, 0.02414, 0.02367,
0.02181, 0.01664, 0.001])

# Flow conditions for hover
v_inf = 0 # Hover condition, set free-stream velocity to 0
Cl = 1.2
Cd = 0.21
```

```
def tip_loss_factor(r, R):
    """Calculate Prandtl's tip loss factor for a given radius"""
    return (2 / np.pi) * np.arccos(np.exp(-np.pi * (1 - r / R)))


def calculate_thrust_and_torque(rho, num_blades, num_sections, radii, chords, omega, v_inf, Cl, Cd):
    total_thrust = 0
    total_torque = 0
    #a = 0.25 # Axial induction factor (typical for hover)

    for i in range(num_sections):
        r = radii[i]
        c = chords[i]

        # Local velocity at the blade element (axial velocity in hover)
        velocity_at_section = np.sqrt((omega * r) ** 2 + v_inf ** 2) # Combine rotational and induced velocities

        # Calculate the lift force (contributes to thrust)
        lift_force = 0.5 * rho * (velocity_at_section ** 2) * Cl * c

        # Apply the tip loss correction
        tip_loss = tip_loss_factor(r, radius) # Tip loss factor at this section

        # Elemental thrust contribution with tip loss correction
        dT = num_blades * lift_force * tip_loss * dr
        total_thrust += dT
```

```
        # Calculate the tangential (torque) force at this section (drag)
        drag_force = 0.5 * rho * (velocity_at_section ** 2) * Cd * c  # Drag force for torque

        # Elemental torque contribution (torque = force x radius)
        dT_torque = num_blades * drag_force * r * dr  # Torque is force times radius
        total_torque += dT_torque

    return total_thrust, total_torque


# Calculate thrust and torque
thrust, torque = calculate_thrust_and_torque(rho, num_blades, num_sections, radii, chords, omega, v_inf, Cl, Cd)
eff = thrust/(torque*omega)

# Print the results
print(f"Total Thrust: {thrust:.4f} N")
print(f"Total Torque: {torque:.4f} N·m")
print(f"Thrust Per Unit Work: {eff:.4f} N/W")
```

GA with BEMT

```
# Import libraries
import numpy as np
import matplotlib.pyplot as plt
import random
# User inputs
diameter_inch = 8 # Diameter of the rotor in inches
rpm = 3000 # Rotations per minute
num_blades = 2 # Number of blades
num_sections = 11 # Number of sections (blade elements)
rho = 1.225 # Air density (kg/m^3)
v_inf = 0 # Free-stream velocity (set to 0 for hover condition)
Cl = 1.2 # Lift coefficient
Cd = 0.21 # Drag coefficient
lower_bound = 0.01 # Lower bound for chord length
upper_bound = 0.025 # Upper bound for chord length
tip_chord = 0.001 # Chord length at the tip
mutation_rate=0.1 # Mutation rate
keep_population_after_selection = 0.8 # The population that remains after every selection
size = 50000 # Number of initial population
target_fitness = 0.19374 # Target fitness for stopping criterion

# Create initial population
def create_initial_population(size, lower_bound, upper_bound, num_sections):
  population = []
  for _ in range(size):
    # Fixed first 3 values
    individual = [0.0112, 0.012, 0.015]

    # Random values for the middle section
    middle_values = [random.uniform(lower_bound, upper_bound) for _ in
```

```
        range(num_sections - 6)]  # Subtract 6 because of 3 fixed at the start and 3 at the end

        # Fixed last 3 values
        individual.extend(middle_values)
        individual.extend([0.015, 0.01, 0.001])  # Last 3 fixed values

        population.append(individual)
    return population

# Convert diameter to meters and compute other properties
diameter = diameter_inch * 0.0254
radius = diameter / 2
dr = radius / (num_sections - 1)  # Correct dr calculation

omega = (2 * np.pi * rpm) / 60

# Radii and chord distribution
radii = np.array(
    [0, 0.1 * radius, 0.2 * radius, 0.3 * radius, 0.4 * radius, 0.5 * radius, 0.6 * radius, 0.7 * radius,
0.8 * radius,
     0.9 * radius, radius])

def tip_loss_factor(r, R):
    """Calculate Prandtl's tip loss factor for a given radius"""
    return (2 / np.pi) * np.arccos(np.exp(-np.pi * (1 - r / R)))

def fitness(rho, num_blades, num_sections, radii, chords, omega, v_inf, Cl, Cd):
    total_thrust = 0
    total_torque = 0
    for i in range(num_sections):
        r = radii[i]
```

```
        c = chords[i]

        # Local velocity at the blade element (axial velocity in hover)
        velocity_at_section = np.sqrt((omega * r) ** 2 + v_inf ** 2)  # Combine rotational and induced velocities
        # Calculate the lift force (contributes to thrust)
        lift_force = 0.5 * rho * (velocity_at_section ** 2) * Cl * c

        # Apply the tip loss correction
        tip_loss = tip_loss_factor(r, radius)  # Tip loss factor at this section

        # Elemental thrust contribution with tip loss correction
        dT = num_blades * lift_force * tip_loss * dr
        total_thrust += dT

        # Calculate the tangential (torque) force at this section (drag)
        drag_force = 0.5 * rho * (velocity_at_section ** 2) * Cd * c  # Drag force for torque

        # Elemental torque contribution (torque = force x radius)
        dT_torque = num_blades * drag_force * r * dr  # Torque is force times radius
        total_torque += dT_torque

    # Calculate efficiency (fitness)
    eff = total_thrust / (total_torque * omega) if total_torque != 0 else 0  # Avoid division by zero
    return eff


# Crossover function (one-point crossover)
def crossover(parent1, parent2):
    # Perform single-point crossover, ensuring the first 3 and last 3 values are preserved
    point = random.randint(3, len(parent1) - 4)  # Choose a random crossover point (not the first or
```

```
    last 3 genes)

    # Create offspring by combining the genes from both parents
    offspring1 = parent1[:point] + parent2[point:]
    offspring2 = parent2[:point] + parent1[point:]

    return offspring1, offspring2

# Mutation function
def mutate(individual, mutation_rate=mutation_rate, lower_bound=lower_bound, upper_bound=upper_bound):
    # Mutation: randomly alter one gene of the individual (excluding fixed values)
    if random.random() < mutation_rate:
        # Choose a random index to mutate from the middle values
        mutation_index = random.randint(3, len(individual) - 4)  # Ensure mutation does not affect the first 3 or last 3
        # Mutate the gene by assigning a new random value within the specified bounds
        individual[mutation_index] = random.uniform(lower_bound, upper_bound)
    return individual
# Selection function
def selection(population, fitness_func):
    # Calculate fitness for each individual
    population_with_fitness = [(individual, fitness_func(rho, num_blades, num_sections, radii, individual, omega, v_inf, Cl, Cd)) for individual in population]

    # Sort the population by fitness values (descending order)
    population_with_fitness.sort(key=lambda x: x[1], reverse=True)

    # Select the top 80% of the population
    cutoff_index = int(len(population_with_fitness) * keep_population_after_selection)
    selected_population = [individual for individual, fitness in
```

```
population_with_fitness[:cutoff_index]]
    return selected_population

# Store fitness over generations
fitness_over_generations = []
# Evolutionary loop until reaching target fitness
generation = 0
best_chords = None  # Variable to store the chords of the best individual
population = create_initial_population(size, lower_bound, upper_bound, num_sections)

while True:
    generation += 1

    # Apply selection to get the top individuals
    selected_population = selection(population, fitness)
    # Generate offspring
    offspring = []
    if len(selected_population) % 2 != 0:  # If the population size is odd
        selected_population = selected_population[:-1] # Remove the last individual to make it even

    for i in range(0, len(selected_population), 2):
        parent1, parent2 = selected_population[i], selected_population[i + 1]
        # Perform crossover to generate two offspring
        offspring1, offspring2 = crossover(parent1, parent2)
        # Apply mutation
        offspring1 = mutate(offspring1)
        offspring2 = mutate(offspring2)
        # Add the offspring to the offspring list
        offspring.append(offspring1)
        offspring.append(offspring2)
```

```
    # Update the population with the new offspring
    population = offspring

    # Calculate the fitness of the current population
    best_fitness = max(fitness(rho, num_blades, num_sections, radii, individual, omega, v_inf, Cl, Cd) for individual in population)
    # Find the individual with the best fitness
    best_individual = max(population, key=lambda individual: fitness(rho, num_blades, num_sections, radii, individual, omega, v_inf, Cl, Cd))
    # Track the chords of the best individual
    best_chords = best_individual[:num_sections] # The first 10 values correspond to chords
    # Record the fitness value
    fitness_over_generations.append(best_fitness)

    # Print the best fitness and the corresponding chords
    print(f"Generation {generation}: Best Fitness = {best_fitness}")
    print(f"Best Chords: {best_chords}")

    # Check if the best fitness reaches the target
    if best_fitness >= target_fitness:
        print(f"Target fitness of {target_fitness} reached in generation {generation}.")
        break
# Plot fitness over generations
plt.plot(fitness_over_generations)
plt.title('Fitness Over Generations')
plt.xlabel('Generation')
plt.ylabel('Fitness')
plt.grid(True)
plt.show()
```